COMUNE DI FINALE LIGURE

Provincia di Savona



Riformulazione del progetto di P.U.O. del sub distretto di trasformazione DT1a - aree ex cava Ghigliazza a seguito del parere del Comitato VIA

committente

CAVA ARENE CANDIDE SRL

Sede legale: Via Ferruccio Ferrari 4 - 42100 Reggio Emilia *Sede operativa:* Via Clementi 16 - 42100 Reggio Emilia

Tel. 0522.306086 Fax. 0522.935164 E.mail: melioli@intertechsrl.com

Presidente e legale rappresentante Giovanni MELIOLI

responsabile progettazione

arch. PierGiorgio CASTELLARI

Piazza del Popolo 3/8, 17100 Savona
tel 019 804597 - fax 019 8486939
e-mail archet@archet.it

arch. Valter CATTANEO

via Garibaldi 17, 17027 Pietra Ligure (SV)
tel 019 625320 - fax 019 629837
e-mail info@architettocattaneo.it

consulenza per le tematiche geologico-geotecniche

ing. Oscar TONELLO

via Ruffini 7/7 18038 Sanremo IM
tel 0184 541130 - fax 0184 541130
e-mail studio.tonello@libero.it

geol. Giorgio CONTI

via Ruffini 7/7 18038 Sanremo IM
tel 0184 541130 - fax 0184 541130
e-mail gio_conti@libero.it

oggetto

RELAZIONE DI CALCOLO
VERIFICHE SEZIONI 2-2 / 5-5 - METODO D.E.M. E F.E.M

elaborato **C3.3**

data settembre 2013

scala --------

cod.	003003	percorso file /dati/.../prj/cava arene candide	redatto	corretto	approvato
rev1	giugno 2013	motivo Riformulazione a seguito parere Comitato VIA	Tonello - Bianchi	Tonello-Conti	Tonello-Conti
rev2	settembre 2013	motivo Integrazione a seguito parere settore VIA del 01/07/13			
rev3		motivo			
rev4		motivo			
rev5		motivo			

SEZIONE 2-2

Analisi di stabilità dei pendii con: DEM (1992)

Zona	Finale Ligure
Lat./Long.	44,1616659/8,326222
Normativa	NTC 2008
Numero di strati	5,0
Numero dei conci	50,0
Grado di sicurezza ritenuto accettabile	1,1
Coefficiente parziale resistenza	1,1
Parametri geotecnici da usare. Angolo di attrito:	Picco
Analisi	Condizione drenata
Superficie di forma generica	

Coefficienti sismici [N.T.C.]

Dati generali

Tipo opera:	2 - Opere ordinarie
Classe d'uso:	Classe II
Vita nominale:	50,0 [anni]
Vita di riferimento:	50,0 [anni]

Parametri sismici su sito di riferimento

Categoria sottosuolo:	A
Categoria topografica:	T4

S.L. Stato limite	TR Tempo ritorno [anni]	ag [m/s²]	F0 [-]	TC* [sec]
S.L.O.	30,0	0,2	2,61	0,16
S.L.D.	50,0	0,03	2,52	0,2
S.L.V.	475,0	0,09	2,51	0,29
S.L.C.	975,0	0,12	2,51	0,3

Coefficienti sismici orizzontali e verticali

Opera: Stabilità dei pendii e Fondazioni

S.L. Stato limite	amax [m/s²]	beta [-]	kh [-]	kv [sec]
S.L.O.	0,28	0,2	0,0057	0,0029
S.L.D.	0,042	0,2	0,0009	0,0004
S.L.V.	0,126	0,2	0,0026	0,0013
S.L.C.	0,168	0,2	0,0034	0,0017

Coefficiente azione sismica orizzontale	0,003
Coefficiente azione sismica verticale	0,001
Intensità di Arias	2,260 m/s
Intensità degli incroci con l'asse dei tempi accelerogramma	0,050 1/s
Durata accelerogramma Trifunac (1975)	12,960 s

Vertici profilo

Nr	X (m)	y (m)
1	0,0	0,0
2	23,6	1,5
3	23,6	6,2
4	44,1	6,2

5	44,1	8,7
6	45,0	9,3
7	63,2	9,3
8	85,0	9,3
9	103,0	9,3
10	103,0	10,6
11	137,0	10,6
12	137,0	20,0
13	145,0	20,0
14	149,0	20,0
15	149,0	26,0
16	151,0	26,0
17	151,0	29,0
18	154,0	29,0
19	154,0	32,0
20	157,0	32,0
21	157,0	35,0
22	160,0	35,0
23	160,0	38,0
24	167,6	38,0
25	173,0	38,0
26	173,0	41,0
27	203,0	41,0
28	203,0	48,0
29	205,0	48,0
30	205,0	51,0
31	211,0	53,0
32	214,0	54,0
33	214,0	56,0
34	223,0	56,0
35	223,0	58,0
36	228,0	58,0
37	228,0	60,0
38	234,9	60,0
39	247,0	61,0
40	261,0	62,0
41	265,0	62,0
42	285,0	78,0
43	296,0	87,0
44	309,0	98,0
45	326,0	111,0
46	355,0	133,0
47	363,6	133,0
48	366,0	139,0
49	367,7	144,0
50	375,0	145,0
51	379,0	152,0
52	385,0	152,0
53	388,0	153,0
54	392,0	162,0
55	396,0	172,0
56	399,0	175,0
57	402,5	175,0
58	405,0	173,0
59	411,0	173,0
60	420,1	197,8
61	428,4	197,8
62	437,6	222,0
63	446,0	222,0
64	455,2	246,0

65	562,1	258,8

Vertici strato 1

N	X (m)	y (m)
1	0,0	0,0
2	23,6	1,5
3	23,6	6,2
4	44,1	6,2
5	44,1	8,7
6	45,0	9,3
7	63,2	9,3
8	85,0	9,3
9	103,0	9,3
10	103,0	10,6
11	137,0	10,6
12	137,0	20,0
13	145,0	20,0
14	149,0	20,0
15	149,0	26,0
16	151,0	26,0
17	151,0	29,0
18	154,0	29,0
19	154,0	32,0
20	157,0	32,0
21	157,0	35,0
22	160,0	35,0
23	160,0	38,0
24	167,6	38,0
25	173,0	38,0
26	173,0	41,0
27	203,0	41,0
28	203,0	48,0
29	205,0	48,0
30	205,0	51,0
31	211,0	53,0
32	214,0	54,0
33	214,0	56,0
34	223,0	56,0
35	223,0	58,0
36	228,0	58,0
37	228,0	60,0
38	234,9	60,0
39	247,0	61,0
40	261,0	62,0
41	265,0	62,0
42	285,0	78,0
43	296,0	87,0
44	309,0	98,0
45	326,0	111,0
46	355,0	133,0
47	363,6	133,0
48	366,0	139,0
49	367,7	144,0
50	375,0	145,0
51	379,0	152,0
52	385,0	152,0
53	388,0	153,0
54	392,0	162,0
55	396,0	172,0
56	399,0	175,0

57	402,5	175,0
58	405,0	173,0
59	411,0	173,0
60	420,1	197,8
61	436,0	196,0
62	562,1	180,0

Vertici strato 2

N	X (m)	y (m)
1	0,0	0,0
2	23,6	1,5
3	23,6	6,2
4	44,1	6,2
5	44,1	8,7
6	45,0	9,3
7	63,2	9,3
8	85,0	9,3
9	103,0	9,3
10	103,0	10,6
11	137,0	10,6
12	137,0	20,0
13	145,0	20,0
14	149,0	20,0
15	149,0	26,0
16	151,0	26,0
17	151,0	29,0
18	154,0	29,0
19	154,0	32,0
20	157,0	32,0
21	157,0	35,0
22	160,0	35,0
23	160,0	38,0
24	167,6	38,0
25	173,0	38,0
26	173,0	41,0
27	203,0	41,0
28	203,0	48,0
29	205,0	48,0
30	205,0	51,0
31	211,0	53,0
32	214,0	54,0
33	214,0	56,0
34	223,0	56,0
35	223,0	58,0
36	228,0	58,0
37	228,0	60,0
38	234,9	60,0
39	247,0	61,0
40	261,0	62,0
41	265,0	62,0
42	285,0	78,0
43	296,0	87,0
44	309,0	98,0
45	326,0	111,0
46	355,0	133,0
47	363,6	133,0
48	366,0	139,0
49	416,0	152,0
50	436,0	196,0
51	436,0	196,0

52	562,1	180,0

Vertici strato 3

N	X (m)	y (m)
1	0,0	0,0
2	23,6	1,5
3	23,6	1,5
4	23,6	6,2
5	44,1	6,2
6	60,0	8,0
7	63,2	9,3
8	85,0	9,3
9	136,0	8,0
10	142,0	16,0
11	145,0	20,0
12	149,0	20,0
13	149,0	26,0
14	151,0	26,0
15	151,0	29,0
16	154,0	29,0
17	154,0	32,0
18	157,0	32,0
19	157,0	35,0
20	160,0	35,0
21	160,0	38,0
22	167,6	38,0
23	173,0	38,0
24	173,0	41,0
25	203,0	41,0
26	203,0	48,0
27	205,0	48,0
28	205,0	51,0
29	211,0	53,0
30	225,0	53,0
31	235,0	56,0
32	262,0	59,0
33	265,0	62,0
34	285,0	78,0
35	296,0	87,0
36	309,0	98,0
37	326,0	111,0
38	355,0	133,0
39	363,6	133,0
40	366,0	139,0
41	416,0	152,0
42	436,0	196,0
43	436,0	196,0
44	562,1	180,0

Vertici strato 4

N	X (m)	y (m)
1	0,0	0,0
2	23,6	1,5
3	23,6	1,5
4	23,6	1,5
5	23,6	1,5
6	23,6	1,5
7	23,6	1,5
8	23,6	1,5
9	23,6	6,2

10	44,1	6,2
11	60,0	8,0
12	63,2	9,3
13	85,0	9,3
14	136,0	8,0
15	142,0	16,0
16	145,0	20,0
17	149,0	20,0
18	149,0	26,0
19	151,0	26,0
20	151,0	29,0
21	154,0	29,0
22	154,0	32,0
23	157,0	32,0
24	157,0	35,0
25	160,0	35,0
26	160,0	38,0
27	167,6	38,0
28	180,0	0,0
29	149,0	0,0
30	142,0	16,0
31	145,0	20,0
32	149,0	20,0
33	149,0	26,0
34	151,0	26,0
35	151,0	29,0
36	154,0	29,0
37	154,0	32,0
38	157,0	32,0
39	157,0	35,0
40	160,0	35,0
41	160,0	38,0
42	167,6	38,0
43	173,0	38,0
44	173,0	41,0
45	203,0	41,0
46	203,0	48,0
47	205,0	48,0
48	205,0	51,0
49	211,0	53,0
50	225,0	53,0
51	235,0	56,0
52	262,0	59,0
53	265,0	62,0
54	285,0	78,0
55	296,0	87,0
56	309,0	98,0
57	326,0	111,0
58	355,0	133,0
59	363,6	133,0
60	366,0	139,0
61	416,0	152,0
62	436,0	196,0
63	436,0	196,0
64	562,1	180,0
65	562,1	0,0

Vertici superficie Nr...1

N	X m	y m

1	186,97	41,09
2	214,0	33,0
3	249,0	30,0
4	284,0	33,0
5	321,0	43,0
6	361,0	61,0
7	393,0	85,0
8	427,0	120,0
9	450,0	147,0
10	469,0	185,0
11	477,0	207,0
12	489,0	233,0
13	496,02	250,96

Coefficienti parziali per i parametri geotecnici del terreno

Tangente angolo di resistenza al taglio	1,25
Coesione efficace	1,25
Coesione non drenata	1,4
Riduzione parametri geotecnici terreno	Si

Stratigrafia

c: coesione; cu: coesione non drenata; Fi: Angolo di attrito; G: Peso Specifico; Gs: Peso Specifico Saturo; K: Modulo di Winkler

Strato	c (kg/cm²)	cu (kg/cm²)	Fi (°)	G (Kg/m³)	Gs (Kg/m³)	Litologia	
1	2		42	2500	2700	Pietra di Finale	
2	1		38	2400	2600	Vedrina	
3	0,2		30	1850	2100	Riempimenti	
4	1,2		36	2450	2650	Facies Pelitica Tanarello	
5	1,5		40	2450	2650	Calcari Tanarello	

G0: Modulo di taglio dinamico a basse deformazioni; G: Modulo di taglio dinamico; Dr: Densità relativa; OCR: Grado di sovraconsolidazione; IP: Indice di plasticità

Strato	G0 (KPa)	G (KPa)	Dr (%)	OCR	IP (%)
1	100000	75000	85	4	40
2	80000	60000	80	3	35
3	60000	45000	70	2	30
4	80000	60000	80	3	35
5	100000	75000	85	4	40

DEM Strato...1

Strato	Coesione (kg/cm²)	Spostamento (mm)	Angolo resistenza al taglio (°)	Spostamento (mm)	Rigidezza normale (KN/m3)	Rigidezza tangenziale (KN/m3)
1	2	1	42	1	200000	100000

DEM Strato...2

Strato	Coesione (kg/cm²)	Spostamento (mm)	Angolo resistenza al taglio (°)	Spostamento (mm)	Rigidezza normale (KN/m3)	Rigidezza tangenziale (KN/m3)

1	1	1	38	1	150000	75000

DEM Strato...3

Strato	Coesione (kg/cm²)	Spostamento (mm)	Angolo resistenza al taglio (°)	Spostamento (mm)	Rigidezza normale (KN/m3)	Rigidezza tangenziale (KN/m3)
1	0,2	1	30	1	100000	50000

DEM Strato...4

Strato	Coesione (kg/cm²)	Spostamento (mm)	Angolo resistenza al taglio (°)	Spostamento (mm)	Rigidezza normale (KN/m3)	Rigidezza tangenziale (KN/m3)
1	1,2	1	36	1	150000	75000

DEM Strato...5

Strato	Coesione (kg/cm²)	Spostamento (mm)	Angolo resistenza al taglio (°)	Spostamento (mm)	Rigidezza normale (KN/m3)	Rigidezza tangenziale (KN/m3)
1	1,5	1	40	1	200000	100000

Pali...

N°	x (m)	y (m)	Diametro (m)	Lunghezza (m)	Inclinazione (°)	Interasse (m)
1	203	48	0,2	10,5	90	0,5
2	149	26	0,2	9	90	0,5
3	137	20	0,2	13,5	90	0,5

Tiranti

N°	x (m)	y (m)	Lunghezza libera (m)	Lunghezza ancorata (m)	Diametro del bulbo (m)	Inclinazione (°)	Tiro (Kg)
1	203	44	8	8	0,25	20	15000
2	203	47	8	8	0,25	20	15000
3	149	22	8	8	0,25	20	15000
4	137	15	8	8	0,25	20	15000
5	137	18	8	8	0,25	20	15000

Carichi distribuiti

N°	xi (m)	yi (m)	xf (m)	yf (m)	Carico esterno (kg/cm²)
1	127	10,6	136	10,6	2
2	180	41	198	41	3
3	142	20	148	20	1,5

Spostamenti

ConcioNr.	Xg (m)	Yg (m)	Ux (m)	Uy (m)	ß (°)
1	191,4093	40,3805	-0,0006	0,0023	--
2	196,8862	39,5621	-0,0004	0,0018	--
3	203,3562	41,6874	-0,0007	0,0016	--
4	209,0052	43,4118	-0,0008	0,0025	--
5	215,1526	43,906	-0,0007	0,0031	--
6	221,2929	44,6961	-0,0006	0,0035	--
7	227,4621	45,4308	-0,0005	0,0038	--
8	233,6003	45,6968	-0,0004	0,0041	--
9	239,78	45,5968	-0,0002	0,0043	--
10	245,9535	45,5826	-0,0001	0,0045	--

11	252,1092	45,8157	0,0002	0,0046	--
12	258,283	46,2942	0,0004	0,0048	--
13	264,483	47,1768	0,0006	0,0051	--
14	270,6984	49,2092	0,0008	0,0056	--
15	276,8652	51,9403	0,0011	0,0062	--
16	283,0291	54,7719	0,0014	0,0068	--
17	289,1927	57,9167	0,0016	0,0074	--
18	295,3645	61,2928	0,0019	0,008	--
19	301,5377	64,7127	0,0021	0,0085	--
20	307,7087	68,1211	0,0024	0,0091	--
21	313,8772	71,4024	0,0027	0,0097	--
22	320,048	74,6911	0,0029	0,0103	--
23	326,215	78,2506	0,0032	0,011	--
24	332,3889	81,9857	0,0035	0,0118	--
25	338,5621	85,7165	0,0038	0,0128	--
26	344,7368	89,4475	0,0041	0,014	--
27	350,9096	93,1784	0,0044	0,0157	--
28	357,0563	95,919	0,0048	0,018	--
29	363,263	99,6658	0,0052	0,0214	--
30	369,4189	104,816	0,0054	0,0248	--
31	375,6076	110,0104	0,0056	0,028	--
32	381,7386	114,1359	0,0059	0,0312	--
33	387,9633	118,5787	0,0061	0,0347	--
34	394,1653	126,542	0,0098	0,0534	--
35	400,2562	133,107	0,0094	0,0567	--
36	406,411	136,2331	0,0096	0,0594	--
37	412,6837	142,3974	0,0095	0,0617	--
38	418,8477	151,7577	0,0087	0,0636	--
39	424,9438	157,8799	0,0083	0,0653	--
40	431,2114	165,2821	0,0078	0,067	--
41	437,3445	174,8734	0,007	0,0681	--
42	443,4738	181,0534	0,0066	0,0687	--
43	449,7217	189,7729	0,0061	0,0692	--
44	455,8237	200,8319	0,0056	0,0687	--
45	461,9532	208,8569	0,0054	0,0663	--
46	468,0969	215,7835	0,0055	0,0626	--
47	474,2098	223,7376	0,006	0,0567	--
48	480,3651	231,6515	0,0067	0,0477	--
49	486,4177	238,6438	0,0076	0,0355	--
50	491,872	245,3676	0,0079	0,0161	--

Sforzi sui conci

Wi (Kg)	Xi (Kg)	Ei (Kg)	Xi-1 (Kg)	Ei-1 (Kg)	Ti (Kg)	Ni (Kg)	Ui (Kg)
196206,0	-16510,76	1188,26	0,0	0,0	-50223,71	172490,0	0,0
178260,4	-14271,58	-360,1	-16510,76	1188,26	-53137,64	172506,5	0,0
69910,99	64073,25	8771,92	-14271,58	-360,1	-33576,82	144705,7	0,0
268674,3	42829,97	33672,52	64073,25	8771,92	-46347,14	244406,7	0,0
334913,5	20230,09	47749,03	42829,97	33672,52	-33141,3	310916,2	0,0
346186,0	25076,73	53852,48	20230,09	47749,03	-22862,66	350360,5	0,0
379718,2	29027,85	62217,15	25076,73	53852,48	-23296,57	383079,3	0,0
417429,3	23291,5	73725,42	29027,85	62217,15	-22445,06	411277,6	0,0
433553,6	22431,05	89505,17	23291,5	73725,42	-19934,65	432571,6	0,0
449898,0	22808,88	113037,8	22431,05	89505,17	-13371,7	450764,3	0,0
457582,6	30141,56	111165,4	22808,88	113037,8	39206,67	463258,1	0,0
457156,0	57649,7	119363,5	30141,56	111165,4	50925,19	482077,7	0,0
462003,8	110752,5	136811,7	57649,7	119363,5	62756,45	511615,9	0,0
524168,9	150037,8	162702,7	110752,5	136811,7	75482,13	559049,7	0,0
590878,8	177806,6	198542,8	150037,8	162702,7	90309,7	613175,3	0,0
654701,8	194886,5	228587,1	177806,6	198542,8	129716,2	659915,9	0,0

711049,3	202606,4	236162,9	194886,5	228587,1	196905,5	691341,4	0,0
762220,8	214607,5	251424,5	202606,4	236162,9	218942,6	742826,1	0,0
815721,0	228088,7	274024,6	214607,5	251424,5	240526,9	793948,6	0,0
869505,0	242327,1	305562,3	228088,7	274024,6	263538,1	844219,5	0,0
917311,4	263469,9	349348,9	242327,1	305562,3	289778,7	893812,9	0,0
960616,4	289712,2	391373,5	263469,9	349348,9	353383,7	922505,0	0,0
995509,9	325884,4	425662,1	289712,2	391373,5	457359,1	925520,7	0,0
1024333,0	401039,0	481011,3	325884,4	425662,1	504465,3	978669,3	0,0
1053157,0	530773,4	560753,8	401039,0	481011,3	561018,1	1044684,0	0,0
1081980,0	740647,4	668591,6	530773,4	560753,8	631427,1	1132482,0	0,0
1110803,0	1070396,0	806854,4	740647,4	668591,6	720272,6	1255557,0	0,0
1115864,0	1603774,0	973768,9	1070396,0	806854,4	832062,0	1434120,0	0,0
1061739,0	1617696,0	1065011,0	1603774,0	973768,9	699210,3	822830,6	0,0
1162217,0	1409659,0	1127798,0	1617696,0	1065011,0	625523,2	723582,8	0,0
1119377,0	1363762,0	1179016,0	1409659,0	1127798,0	687748,1	826034,3	0,0
1138172,0	1447289,0	1217748,0	1363762,0	1179016,0	766742,3	952073,1	0,0
1083150,0	2149881,0	1238172,0	1447289,0	1217748,0	1090381,0	1414389,0	0,0
1216740,0	1547466,0	1088527,0	2149881,0	1238172,0	559102,1	621563,3	0,0
1239524,0	992359,0	1058603,0	1547466,0	1088527,0	472667,4	495704,2	0,0
1114243,0	691207,9	1004563,0	992359,0	1058603,0	547890,8	602910,6	0,0
1084742,0	595228,7	915788,3	691207,9	1004563,0	649637,1	750302,2	0,0
1240111,0	523139,6	789601,9	595228,7	915788,3	752446,1	901692,2	0,0
1199343,0	536382,9	638745,3	523139,6	789601,9	778549,6	941224,3	0,0
1211980,0	216474,2	510057,8	536382,9	638745,3	598019,1	673697,4	0,0
1356703,0	-52554,96	328574,0	216474,2	510057,8	712910,0	840351,2	0,0
1258090,0	82185,53	64098,5	-52554,96	328574,0	891221,1	1101658,0	0,0
1279680,0	-573590,3	-65159,21	82185,53	64098,5	455563,8	444372,5	0,0
1337776,0	-1449076,0	-160905,0	-573590,3	-65159,21	372435,7	288774,5	0,0
1162641,0	-1966510,0	-270222,1	-1449076,0	-160905,0	407662,5	338211,4	0,0
974503,5	-2448676,0	-391551,9	-1966510,0	-270222,1	403230,0	306284,6	0,0
750767,1	-2549271,0	-537885,4	-2448676,0	-391551,9	559918,7	360527,5	0,0
529998,6	-2302155,0	-740156,6	-2549271,0	-537885,4	621490,1	507866,5	0,0
332460,6	-2006910,0	-865282,6	-2302155,0	-740156,6	521243,0	371118,2	0,0
116229,0	1073,81	1926,04	-2006910,0	-865282,6	2292577,0	-33481,96	0,0

Superficie Nr...1 Fattore di sicurezza=1,32

Analisi di stabilità dei pendii con: FEM metodo ZENG LIANG (1995)

Zona	Finale Ligure
Lat./Long.	44,1616659/8,326222
Normativa	NTC 2008
Numero di strati	5,0
Numero dei conci	50,0
Grado di sicurezza ritenuto accettabile	1,1
Coefficiente parziale resistenza	1,1
Parametri geotecnici da usare. Angolo di attrito:	Picco
Superficie di forma generica	

Coefficienti sismici [N.T.C.]

Dati generali

Tipo opera:	2 - Opere ordinarie
Classe d'uso:	Classe II
Vita nominale:	50,0 [anni]
Vita di riferimento:	50,0 [anni]

Parametri sismici su sito di riferimento

Categoria sottosuolo:	A
Categoria topografica:	T4

S.L. Stato limite	TR Tempo ritorno [anni]	ag [m/s²]	F0 [-]	TC* [sec]
S.L.O.	30,0	0,2	2,61	0,16
S.L.D.	50,0	0,03	2,52	0,2
S.L.V.	475,0	0,09	2,51	0,29
S.L.C.	975,0	0,12	2,51	0,3

Coefficienti sismici orizzontali e verticali

Opera: Stabilità dei pendii e Fondazioni

S.L. Stato limite	amax [m/s²]	beta [-]	kh [-]	kv [sec]
S.L.O.	0,28	0,2	0,0057	0,0029
S.L.D.	0,042	0,2	0,0009	0,0004
S.L.V.	0,126	0,2	0,0026	0,0013
S.L.C.	0,168	0,2	0,0034	0,0017

Coefficiente azione sismica orizzontale	0,003
Coefficiente azione sismica verticale	0,001
Intensità di Arias	2,260 m/s
Intensità degli incroci con l'asse dei tempi accelerogramma	0,050 1/s
Durata accelerogramma Trifunac (1975)	12,960 s

Coefficienti parziali per i parametri geotecnici del terreno

Tangente angolo di resistenza al taglio	1,25
Coesione efficace	1,25
Coesione non drenata	1,4
Riduzione parametri geotecnici terreno	Si

Stratigrafia

Strato	Peso unità di volume (Kg/m³)	A	B	T	Resistenza compressione monoassiale (kg/cm²)	Texture	Descrizione
1	2500	0,369	0,669	-0,006	750		Pietra di Finale
2	2400	0,369	0,669	-0,006	750		Vedrina
3	1850	0,115	0,646	-0,0002	300		Riempimenti
4	2450	0,198	0,662	-0,0007	450		Facies Pelitica Tanarello
5	2450	0,369	0,669	-0,006	650		Calcari Tanarello

G0: Modulo di taglio dinamico a basse deformazioni; G: Modulo di taglio dinamico; Dr: Densità relativa; OCR: Grado di sovraconsolidazione; IP: Indice di plasticità

Strato	G0 (KPa)	G (KPa)	Dr (%)	OCR	IP (%)
1	100000	75000	85	4	40
2	80000	60000	80	3	35
3	60000	45000	70	2	30
4	80000	60000	80	3	35
5	100000	75000	85	4	40

Pali...

N°	x (m)	y (m)	Diametro (m)	Lunghezza (m)	Inclinazione (°)	Interasse (m)
1	203	48	0,2	10,5	90	0,5
2	149	26	0,2	9	90	0,5
3	137	20	0,2	13,5	90	0,5

Tiranti

N°	x (m)	y (m)	Lunghezza libera (m)	Lunghezza ancorata (m)	Diametro del bulbo (m)	Inclinazione (°)	Tiro (Kg)
1	203	44	8	8	0,25	20	15000
2	203	47	8	8	0,25	20	15000
3	149	22	8	8	0,25	20	15000
4	137	15	8	8	0,25	20	15000
5	137	18	8	8	0,25	20	15000

Carichi distribuiti

N°	xi (m)	yi (m)	xf (m)	yf (m)	Carico esterno (kg/cm²)
1	127	10,6	136	10,6	2
2	180	41	198	41	3
3	142	20	148	20	1,5

Superficie Nr...1 Fattore di sicurezza=1,37

SEZIONE 5-5

Analisi di stabilità dei pendii con: DEM (1992)

Zona	Finale Ligure
Lat./Long.	44,164278/8,332983
Normativa	NTC 2008
Numero di strati	4,0
Numero dei conci	50,0
Grado di sicurezza ritenuto accettabile	1,1
Coefficiente parziale resistenza	1,0
Parametri geotecnici da usare. Angolo di attrito:	Picco
Analisi	Condizione drenata
Superficie di forma generica	

Coefficienti sismici [N.T.C.]

Dati generali

Tipo opera:	2 - Opere ordinarie
Classe d'uso:	Classe II
Vita nominale:	50,0 [anni]
Vita di riferimento:	50,0 [anni]

Parametri sismici su sito di riferimento

Categoria sottosuolo:	A
Categoria topografica:	T4

S.L. Stato limite	TR Tempo ritorno [anni]	ag [m/s²]	F0 [-]	TC* [sec]
S.L.O.	30,0	0,19	2,62	0,16
S.L.D.	50,0	0,26	2,52	0,2
S.L.V.	475,0	0,8	2,52	0,29
S.L.C.	975,0	1,1	2,52	0,31

Coefficienti sismici orizzontali e verticali

Opera: Stabilità dei pendii e Fondazioni

S.L. Stato limite	amax [m/s²]	beta [-]	kh [-]	kv [sec]
S.L.O.	0,266	0,2	0,0054	0,0027
S.L.D.	0,364	0,2	0,0074	0,0037
S.L.V.	1,12	0,2	0,0228	0,0114
S.L.C.	1,54	0,27	0,0424	0,0212

Coefficiente azione sismica orizzontale	0,023
Coefficiente azione sismica verticale	0,011
Intensità di Arias	2,260 m/s
Intensità degli incroci con l'asse dei tempi accelerogramma	0,050 1/s
Durata accelerogramma Trifunac (1975)	12,960 s

Vertici profilo

Nr	X (m)	y (m)
1	0,0	0,0
2	22,81	2,01
3	22,81	9,55
4	37,99	9,55

5	37,99	12,54
6	44,77	12,55
7	44,77	15,0
8	62,56	15,04
9	70,02	15,2
10	73,2	16,64
11	73,21	16,64
12	73,21	9,1
13	130,62	9,1
14	130,62	17,5
15	134,39	17,5
16	134,39	25,0
17	142,39	25,0
18	142,39	30,66
19	144,23	31,01
20	144,85	31,76
21	145,3	32,43
22	145,78	33,5
23	147,3	40,01
24	148,85	44,71
25	152,68	58,08
26	156,46	70,01
27	157,35	70,01
28	162,7	72,69
29	162,7	73,05
30	164,7	73,05
31	164,7	73,45
32	165,82	73,45
33	166,35	75,01
34	167,5	75,01
35	174,46	78,49
36	175,81	78,08
37	176,5	79,99
38	179,76	80,91
39	179,76	81,16
40	181,26	81,16

Vertici strato 1

N	X (m)	y (m)
1	0,0	0,0
2	22,81	2,01
3	22,81	9,55
4	37,99	9,55
5	51,27	9,56
6	57,86	9,56
7	58,41	12,01
8	66,57	12,01
9	70,02	15,2
10	73,2	16,64
11	73,21	16,64
12	73,21	9,1
13	130,62	9,1
14	130,62	17,5
15	134,39	17,5
16	134,39	25,0
17	142,39	25,0
18	142,39	30,66
19	144,23	31,01
20	144,85	31,76
21	145,3	32,43

22	145,78	33,5
23	147,3	40,01
24	148,85	44,71
25	152,68	58,08
26	156,46	70,01
27	157,35	70,01
28	164,65	70,01
29	165,82	73,45
30	166,35	75,01
31	167,5	75,01
32	174,7	75,01
33	175,81	78,08
34	176,5	79,99
35	179,76	80,91
36	179,76	81,16
37	181,26	81,16

Vertici strato 2

N	X (m)	y (m)
1	0,0	0,0
2	22,81	2,01
3	22,81	3,08
4	33,61	4,87
5	42,31	7,01
6	51,27	9,56
7	57,86	9,56
8	58,41	12,01
9	66,57	12,01
10	70,02	15,2
11	73,2	16,64
12	73,21	16,64
13	73,21	9,1
14	130,62	9,1
15	130,62	17,5
16	134,39	17,5
17	134,39	25,0
18	142,39	25,0
19	142,39	30,66
20	144,23	31,01
21	144,85	31,76
22	145,3	32,43
23	145,78	33,5
24	147,3	40,01
25	148,85	44,71
26	152,68	58,08
27	156,46	70,01
28	157,35	70,01
29	164,65	70,01
30	165,82	73,45
31	166,35	75,01
32	167,5	75,01
33	174,7	75,01
34	175,81	78,08
35	176,5	79,99
36	179,76	80,91
37	179,76	81,16
38	181,26	81,16

Vertici strato 3

N	X (m)	y (m)

1	0,0	0,0
2	105,88	0,0
3	115,35	3,94
4	120,25	9,1
5	130,62	9,1
6	130,62	17,5
7	134,39	17,5
8	134,39	25,0
9	142,39	25,0
10	142,39	30,66
11	144,23	31,01
12	144,85	31,76
13	145,3	32,43
14	154,41	35,76
15	162,51	39,36
16	172,72	42,66
17	181,26	44,71
18	181,26	81,16

Vertici superficie Nr...1

N	X m	y m
1	120,0	9,19
2	131,0	8,0
3	147,0	10,0
4	156,0	18,0
5	162,0	30,0
6	167,0	41,0
7	171,0	52,0
8	174,0	63,0
9	176,0	71,0
10	178,02	80,49

Coefficienti parziali per i parametri geotecnici del terreno

Tangente angolo di resistenza al taglio	1,25
Coesione efficace	1,25
Coesione non drenata	1,4
Riduzione parametri geotecnici terreno	Si

Stratigrafia

c: coesione; cu: coesione non drenata; Fi: Angolo di attrito; G: Peso Specifico; Gs: Peso Specifico Saturo; K: Modulo di Winkler

Strato	c (kg/cm²)	cu (kg/cm²)	Fi (°)	G (Kg/m³)	Gs (Kg/m³)	Litologia	
1	0.10		28	1800	2000	Riporti addensati	
2	0,01		30	1850	2050	Sabbie marine	
3	1,5		40	2450	2650	Calcari Val Tanarello	
4	1,2		36	2450	2650	Facies Pelitica Tanarello	

G0: Modulo di taglio dinamico a basse deformazioni; G: Modulo di taglio dinamico; Dr: Densità relativa; OCR: Grado di sovraconsolidazione; IP: Indice di plasticità

Strato	G0	G	Dr	OCR	IP

	(KPa)	(KPa)	(%)		(%)
1	30000	22500	50	2	35
2	50000	37500	60	2	35
3	100000	75000	85	4	40
4	80000	60000	80	3	35

DEM Strato...1

Strato	Coesione (kg/cm²)	Spostamento (mm)	Angolo resistenza al taglio (°)	Spostamento (mm)	Rigidezza normale (KN/m3)	Rigidezza tangenziale (KN/m3)
1	0,15	1	32	1	50000	25000

DEM Strato...2

Strato	Coesione (kg/cm²)	Spostamento (mm)	Angolo resistenza al taglio (°)	Spostamento (mm)	Rigidezza normale (KN/m3)	Rigidezza tangenziale (KN/m3)
1	0,01	1	33	1	50000	25000

DEM Strato...3

Strato	Coesione (kg/cm²)	Spostamento (mm)	Angolo resistenza al taglio (°)	Spostamento (mm)	Rigidezza normale (KN/m3)	Rigidezza tangenziale (KN/m3)
1	1,5	1	40	1	150000	75000

DEM Strato...4

Strato	Coesione (kg/cm²)	Spostamento (mm)	Angolo resistenza al taglio (°)	Spostamento (mm)	Rigidezza normale (KN/m3)	Rigidezza tangenziale (KN/m3)
1	1,2	1	36	1	150000	75000

Pali...

N°	x (m)	y (m)	Diametro (m)	Lunghezza (m)	Inclinazione (°)	Interasse (m)
1	142,5	31,5	0,2	8	90	0,5
2	134	25	0,2	11	90	0,5
3	131	17,50302	0,2	12,5	90	0,5

Tiranti

N°	x (m)	y (m)	Lunghezza libera (m)	Lunghezza ancorata (m)	Diametro del bulbo (m)	Inclinazione (°)	Tiro (Kg)
1	143	26	8	8	0,25	20	20000
2	143	30	8	8	0,25	20	20000
3	134	24	8	8	0,25	20	20000
4	134	21	8	8	0,25	20	20000
5	134	19	8	8	0,25	20	20000
6	131	16	8	8	0,25	20	20000
7	131	11	8	8	0,25	20	20000

Carichi distribuiti

N°	xi (m)	yi (m)	xf (m)	yf (m)	Carico esterno (kg/cm²)
1	75	9,15	130	9,15	5
2	130,58	17,61	133,58	17,61	1,5
3	134,37	24,93	141,87	24,93	3

Spostamenti

ConcioNr.	Xg (m)	Yg (m)	Ux (m)	Uy (m)	ß (°)
1	121,6383	9,0586	-0,0006	0,0061	--
2	122,6206	9,0068	-0,0006	0,0052	--
3	123,7381	8,946	-0,0006	0,0051	--
4	124,8706	8,8845	-0,0006	0,0051	--
5	126,0083	8,8228	-0,0005	0,0051	--
6	127,1482	8,7609	-0,0004	0,0051	--
7	128,2883	8,6989	-0,0002	0,0051	--
8	129,4304	8,637	0,0001	0,0047	--
9	130,714	11,2441	0,0005	0,0033	--
10	131,7029	12,7955	0,0006	0,0038	--
11	132,846	12,8669	0,0007	0,0043	--
12	134,0455	14,9953	0,0008	0,0049	--
13	135,133	16,7599	0,0008	0,0055	--
14	136,2767	16,8314	0,0009	0,0059	--
15	137,4203	16,9028	0,0009	0,0062	--
16	138,5636	16,9743	0,0011	0,0064	--
17	139,707	17,0458	0,0012	0,0064	--
18	140,8503	17,1173	0,0013	0,0064	--
19	142,0224	18,681	0,0015	0,0063	--
20	143,1379	20,1554	0,0017	0,0064	--
21	144,2844	20,4984	0,0018	0,0066	--
22	145,4348	21,4584	0,002	0,0069	--
23	146,5844	23,4692	0,0021	0,0074	--
24	147,72	25,9069	0,0022	0,0078	--
25	148,8624	28,263	0,0023	0,0082	--
26	150,0058	30,7028	0,0023	0,0086	--
27	151,1492	33,2063	0,0023	0,0089	--
28	152,2916	35,6949	0,0022	0,0092	--
29	153,4331	38,0852	0,0022	0,0093	--
30	154,576	40,3968	0,0021	0,0094	--
31	155,7182	42,7875	0,0021	0,0093	--
32	156,8537	44,7298	0,002	0,0091	--
33	157,9974	46,1645	0,002	0,0089	--
34	159,1408	47,5936	0,0019	0,0086	--
35	160,284	49,0225	0,0019	0,0083	--
36	161,4271	50,4517	0,0018	0,0079	--
37	162,5701	51,9728	0,0017	0,0075	--
38	163,7127	53,4088	0,0017	0,0071	--
39	164,8561	54,7659	0,0016	0,0066	--
40	166,0025	56,5151	0,0015	0,0061	--
41	167,1399	58,283	0,0014	0,0056	--
42	168,2835	59,9658	0,0013	0,0051	--
43	169,425	61,822	0,0012	0,0045	--
44	170,5688	63,7121	0,0011	0,004	--
45	171,7059	65,8508	0,001	0,0034	--
46	172,8463	68,2267	0,0009	0,0028	--
47	173,984	70,6186	0,0008	0,0022	--
48	175,1078	72,8618	0,0006	0,0017	--
49	176,2489	75,6463	0,0005	0,0011	--
50	177,2463	78,521	0,0003	0,0007	--

Sforzi sui conci

Wi (Kg)	Xi (Kg)	Ei (Kg)	Xi-1 (Kg)	Ei-1 (Kg)	Ti (Kg)	Ni (Kg)	Ui (Kg)
52341,84	-2711,3	-221,51	0,0	0,0	-5483,15	49338,04	0,0
57689,81	-1298,89	-114,89	-2711,3	-221,51	-6264,41	58769,4	0,0
58037,71	-1031,53	-13,1	-1298,89	-114,89	-6175,17	57977,31	0,0

58385,61	-812,96	142,55	-1031,53	-13,1	-6145,97	58281,29	0,0
58733,51	-623,79	523,81	-812,96	142,55	-5948,12	58623,17	0,0
59081,41	-211,8	1447,94	-623,79	523,81	-5462,05	59250,03	0,0
59429,31	221,31	3090,47	-211,8	1447,94	-4779,79	59695,29	0,0
59777,21	-4795,26	4203,26	221,31	3090,47	-4747,56	54567,07	0,0
11748,12	22098,96	8405,64	-4795,26	4203,26	1113,55	38861,53	0,0
43524,01	21907,17	9355,67	22098,96	8405,64	6919,32	42804,63	0,0
43123,66	27794,42	10886,22	21907,17	9355,67	8190,49	48368,25	0,0
33760,25	50348,13	12284,44	27794,42	10886,22	8956,01	55632,84	0,0
80482,73	33431,54	13195,7	50348,13	12284,44	9842,64	62830,64	0,0
80082,43	21868,83	13889,76	33431,54	13195,7	10232,22	67773,59	0,0
81962,27	11685,6	20552,44	21868,83	13889,76	10333,86	71046,09	0,0
79281,86	5830,09	20916,35	11685,6	20552,44	10495,17	72685,92	0,0
78881,56	1004,8	21366,07	5830,09	20916,35	10649,31	73301,48	0,0
78481,27	-3666,57	22108,31	1004,8	21366,07	10899,57	73021,81	0,0
57202,29	11861,63	23465,8	-3666,57	22108,31	11367,54	71875,48	0,0
59600,16	25655,96	25554,48	11861,63	23465,8	12535,93	72398,7	0,0
59974,0	41305,25	28827,07	25655,96	25554,48	13996,05	74462,55	0,0
64162,57	56648,1	33291,93	41305,25	28827,07	15756,55	78154,7	0,0
75256,77	64825,89	35661,71	56648,1	33291,93	21786,36	80643,55	0,0
85765,88	64886,18	30386,02	64825,89	35661,71	54551,75	66341,91	0,0
92621,8	62466,99	25409,81	64886,18	30386,02	57799,55	69308,96	0,0
100961,2	55879,75	20061,16	62466,99	25409,81	60436,71	72546,33	0,0
109300,7	44632,05	13899,32	55879,75	20061,16	62416,47	75709,32	0,0
117640,1	28020,15	6604,11	44632,05	13899,32	63689,06	78558,14	0,0
125274,4	5845,73	-2039,62	28020,15	6604,11	64188,21	80885,67	0,0
132534,7	-22590,1	-12201,76	5845,73	-2039,62	63842,6	82530,69	0,0
139349,5	-53898,45	-22127,4	-22590,1	-12201,76	77668,95	75402,61	0,0
141076,0	-63885,97	-19835,71	-53898,45	-22127,4	119480,2	54162,83	0,0
135147,0	-70925,59	-20596,19	-63885,97	-19835,71	115632,3	55190,88	0,0
129917,9	-76527,8	-23042,67	-70925,59	-20596,19	111433,4	55111,51	0,0
124688,9	-81374,21	-26662,33	-76527,8	-23042,67	106854,4	54267,54	0,0
119458,9	-86062,2	-31172,71	-81374,21	-26662,33	101871,5	52892,82	0,0
113908,7	-84634,63	-33608,92	-86062,2	-31172,71	105073,8	47559,48	0,0
107745,6	-83378,7	-36719,36	-84634,63	-33608,92	98969,92	45680,97	0,0
101979,2	-83098,17	-40339,86	-83378,7	-36719,36	92566,13	43475,95	0,0
98530,34	-86522,42	-44570,76	-83098,17	-40339,86	85767,88	41143,38	0,0
93795,1	-84101,48	-46080,16	-86522,42	-44570,76	89794,27	34569,61	0,0
86133,07	-78208,08	-46369,57	-84101,48	-46080,16	87063,91	29859,43	0,0
78501,88	-74550,98	-47187,96	-78208,08	-46369,57	77549,82	27149,59	0,0
70678,3	-71132,0	-47620,45	-74550,98	-47187,96	70364,3	23252,53	0,0
61386,76	-56390,08	-43260,53	-71132,0	-47620,45	74965,09	14462,4	0,0
50819,68	-44433,94	-38581,58	-56390,08	-43260,53	62102,4	10875,68	0,0
39981,84	-32636,14	-32367,07	-44433,94	-38581,58	51904,59	6159,2	0,0
28394,5	-20837,09	-24331,6	-32636,14	-32367,07	41100,77	1319,28	0,0
19479,49	-10689,3	-12123,77	-20837,09	-24331,6	31661,89	-5955,82	0,0
7055,31	32,91	40,05	-10689,3	-12123,77	19918,15	-8311,73	0,0

Superficie Nr...1 Fattore di sicurezza=1,33

Analisi di stabilità dei pendii con: FEM metodo ZENG LIANG (1995)

Zona	Finale Ligure
Lat./Long.	44,164278/8,332983
Normativa	NTC 2008
Numero di strati	4,0
Numero dei conci	50,0
Grado di sicurezza ritenuto accettabile	1,1
Coefficiente parziale resistenza	1,0
Parametri geotecnici da usare. Angolo di attrito:	Picco
Superficie di forma generica	

Coefficienti sismici [N.T.C.]

Dati generali

Tipo opera:	2 - Opere ordinarie
Classe d'uso:	Classe II
Vita nominale:	50,0 [anni]
Vita di riferimento:	50,0 [anni]

Parametri sismici su sito di riferimento

Categoria sottosuolo:	A
Categoria topografica:	T4

S.L. Stato limite	TR Tempo ritorno [anni]	ag [m/s²]	F0 [-]	TC* [sec]
S.L.O.	30,0	0,19	2,62	0,16
S.L.D.	50,0	0,26	2,52	0,2
S.L.V.	475,0	0,8	2,52	0,29
S.L.C.	975,0	1,1	2,52	0,31

Coefficienti sismici orizzontali e verticali

Opera: Stabilità dei pendii e Fondazioni

S.L. Stato limite	amax [m/s²]	beta [-]	kh [-]	kv [sec]
S.L.O.	0,266	0,2	0,0054	0,0027
S.L.D.	0,364	0,2	0,0074	0,0037
S.L.V.	1,12	0,2	0,0228	0,0114
S.L.C.	1,54	0,27	0,0424	0,0212

Coefficiente azione sismica orizzontale	0,023
Coefficiente azione sismica verticale	0,011
Intensità di Arias	2,260 m/s
Intensità degli incroci con l'asse dei tempi accelerogramma	0,050 1/s
Durata accelerogramma Trifunac (1975)	12,960 s

Coefficienti parziali per i parametri geotecnici del terreno

Tangente angolo di resistenza al taglio	1,25
Coesione efficace	1,25
Coesione non drenata	1,4
Riduzione parametri geotecnici terreno	Si

Stratigrafia

Strato	Peso unità di volume (Kg/m³)	A	B	T	Resistenza compressione monoassiale (kg/cm²)	Texture	Descrizione
1	1800	0,115	0,646	-0,0002	300		Riporti addensati
2	1850	0,115	0,646	-0,0002	350		Sabbie marine
3	2450	0,198	0,662	-0,0007	650		Calcari Val Tanarello
4	2450	0,369	0,669	-0,006	450		Facies Pelitica Tanarello

G0: Modulo di taglio dinamico a basse deformazioni; G: Modulo di taglio dinamico; Dr: Densità relativa; OCR: Grado di sovraconsolidazione; IP: Indice di plasticità

Strato	G0 (KPa)	G (KPa)	Dr (%)	OCR	IP (%)
1	30000	22500	50	2	35
2	50000	37500	60	2	35
3	100000	75000	85	4	40
4	80000	60000	80	3	35

Pali...

N°	x (m)	y (m)	Diametro (m)	Lunghezza (m)	Inclinazione (°)	Interasse (m)
1	142,5	31,5	0,2	8	90	0,5
2	134	25	0,2	11	90	0,5
3	131	17,50302	0,2	12,5	90	0,5

Tiranti

N°	x (m)	y (m)	Lunghezza libera (m)	Lunghezza ancorata (m)	Diametro del bulbo (m)	Inclinazione (°)	Tiro (Kg)
1	143	26	8	8	0,25	20	20000
2	143	30	8	8	0,25	20	20000
3	134	24	8	8	0,25	20	20000
4	134	21	8	8	0,25	20	20000
5	134	19	8	8	0,25	20	20000
6	131	16	8	8	0,25	20	20000
7	131	11	8	8	0,25	20	20000

Carichi distribuiti

N°	xi (m)	yi (m)	xf (m)	yf (m)	Carico esterno (kg/cm²)
1	75	9,15	130	9,15	5
2	130,58	17,61	133,58	17,61	1,5
3	134,37	24,93	141,87	24,93	3

Superficie Nr...1 Fattore di sicurezza=1.41

D.E.M.

Interfacciamento tra i blocchi

Con questo metodo il terreno viene modellato come una serie di elementi discreti, che in seguito chiameremo "blocchi", e tiene conto della mutua compatibilità tra i blocchi stessi. A questo scopo ogni blocco e i blocchi adiacenti e la base sono vincolate da molle alla Winkler. Vi sono una serie di molle nella direzione normale all'interfaccia per simulare *la rigidezza normale* e una serie di molle nella direzione tangenziale per simulare la *resistenza allo scorrimento dell'interfaccia*. Il comportamento delle molle normali e di quelle trasversali, è assunto di tipo *elasto-plastico perfetto*. Le molle normali non cedono in compressione ma cedono solo a trazione con una capacità estensionale massima per terreno dotato di coesione e senza capacità estensionale per terreni non coesivi.

Le molle trasversali cedono quando è raggiunta la *massima resistenza a taglio* ed occorre distinguere due tipi di comportamenti diversi: terreno fragile e terreno non fragile. Per terreno fragile la resistenza di picco delle molle a taglio è data da:

$$\tau_p = c_p + \sigma_n \tan\varphi_p$$

τ

Mentre la resistenza residua

$$\tau_r = c_r + \sigma_n \tan\varphi_r$$

Per semplicità nella seguente analisi si è assunto che dopo il raggiungimento della resistenza di picco, la resistenza del terreno si abbatte immediatamente al valore della resistenza residua.

Per terreno non fragile la resistenza non si riduce per grandi deformazioni a taglio, quindi la resistenza residua è uguale a quella di picco.

La formulazione del metodo esposto segue quello di una precedente ricerca svolta da *Chang e Mistra* sulla meccanica dei particolari discreti.

Posti u_i^a, u_i^b, e w^a, w^b in modo che essi rappresentano rispettivamente lo spostamento e la rotazione dei blocchi A e B, si prende il punto P in modo che sia il punto medio dell'interfaccia tra i due blocchi, come mostrato in Fig. 7.1.1. Detto r_i^{ap} il vettore congiungente il baricentro del blocco A con il punto P. Lo spostamento del blocco B relativo al blocco A, nel punto P, è
allora espresso come segue:

$$\begin{Bmatrix} \Delta_x^p \\ \Delta_y^p \\ \Delta_\omega^p \end{Bmatrix} = \begin{bmatrix} 1 & 0 & -r_y^{bp} \\ 0 & 1 & r_x^{bp} \\ 0 & 0 & 1 \end{bmatrix} \cdot \begin{Bmatrix} u_x^b \\ u_y^b \\ \omega^b \end{Bmatrix} - \begin{bmatrix} 1 & 0 & -r_y^{ap} \\ 0 & 1 & r_x^{ap} \\ 0 & 0 & 1 \end{bmatrix} \cdot \begin{Bmatrix} u_x^a \\ u_y^a \\ \omega^a \end{Bmatrix} \quad (3)$$

Se il blocco B è comunque immobile, i valori di u_x^b, u_y^b, e w^b sono assunti pari a zero.

Prendiamo n_i^p in modo che esso sia il vettore normale sulla faccia del blocco A nel punto P, verso l'interno definito da

n_i^p = *(cosa , sina)* dove *a* è l'angolo tra l'asse *X* e il vettore n_i^p. Il vettore s_i^p, perpendicolare al vettore n_i^p, sarà definito da s_i^p = *(-sina, cosa).*

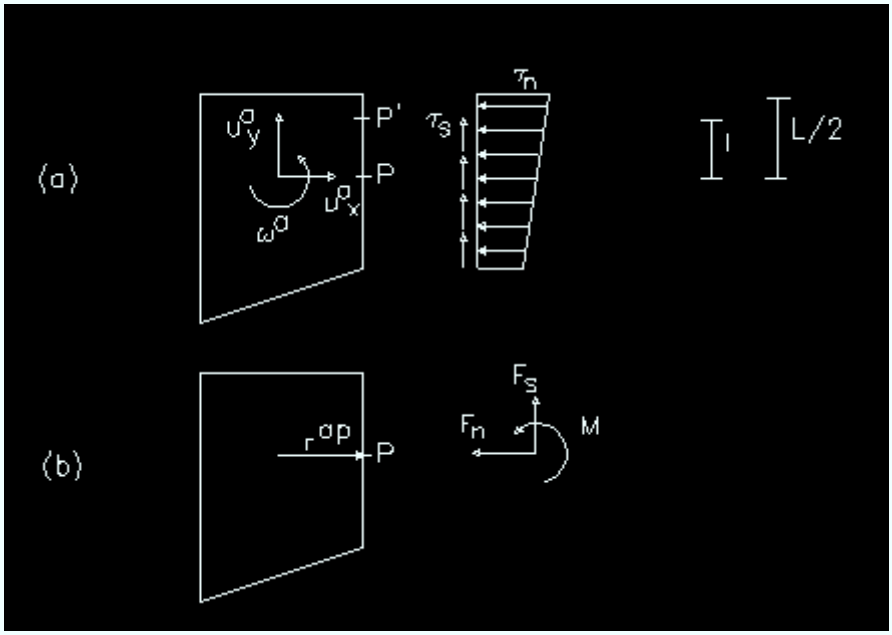


Figura 7.1.1- *(a) tensioni normali e tangenziali ; (b)Forze e momenti equivalenti all'interfaccia.*

ll vettore spostamento del primo membro dell'Eq. 3 può essere trasformato dalle coordinate X-Y nelle coordinate locali n-s come segue:

$$\begin{Bmatrix} \Delta_n^p \\ \Delta^p s \\ \Delta_\omega^p \end{Bmatrix} = \begin{bmatrix} \cos\alpha & \sin\alpha & 0 \\ -\sin\alpha & \cos\alpha & 0 \\ 0 & 0 & 1 \end{bmatrix} \cdot \begin{Bmatrix} \Delta_x^p \\ \Delta^p y \\ \Delta_\omega^p \end{Bmatrix} \quad (4)$$

A causa dello spostamento relativo tra due blocchi vicini, per un generico punto P' dell'interfaccia, distante *l* dal punto centrale P come evidenziato nella Fig. X.Y.1, l'allungamento della molla nella direzione normale d_n e quello nella direzione tangenziale d_s sono date da:

$$d_n = D_n + l \times d_n \qquad d_s = D_s \quad (5)$$

Per effetto dell'allungamento delle molle insorgono tensioni normali e tangenziali in accordo con il comportamento alla Winkler, come mostrato in Fig. X.Y.1. Tali tensioni sull'interfaccia possono essere integrate per ottenere forze e momenti risultanti equivalenti nel modo seguente:

$$F_n = \int_{-L/2}^{L/2} k_n \cdot \delta_n \cdot dl = \int_{-L/2}^{L/2} k_n \cdot \Delta_n \cdot dl + \int_{-L/2}^{L/2} k_n \cdot l \cdot \Delta_\omega \cdot dl \quad (6)$$

$$F_s = \int_{-L/2}^{L/2} k_s \cdot \delta_s \cdot dl = \int_{-L/2}^{L/2} k_s \cdot \Delta_s \cdot dl \quad (7)$$

$$M = \int_{-L/2}^{L/2} k_n \cdot l \cdot \delta_s \cdot dl = \int_{-L/2}^{L/2} k_n \cdot l \cdot \Delta_n \cdot dl + \int_{-L/2}^{L/2} k_n \cdot l^2 \cdot \Delta_\omega \cdot dl \quad (8)$$

dove

k_n = costante della molla normale per unità di lunghezza

k_s = costante della molla trasversale per unità di lunghezza

L = lunghezza dell'interfaccia

Occorre notare che le molle sono di tipo *elasto-plastico* quindi i valori di k_n e k_s sono funzione della deformazione, quindi dovrebbero essere ottenute dalle curve sforzi - deformazioni rappresentate in Fig. X.Y.2. Per le interfaccie che non cedono, vengono usate le costanti elastiche k_n e k_s . Per quelle che cedono le costanti elastiche non possono essere utilizzate, quindi è richiesto un metodo per considerare la non linearità del problema. A tal proposito viene impiegato *il metodo della rigidezza secante.* Le costanti equivalenti $` k_n$ e $` k_s$ possono essere ottenute come quelle corrispondenti alla deformazione dell'interfaccia, come evidenziato in Fig. 7.1.2.

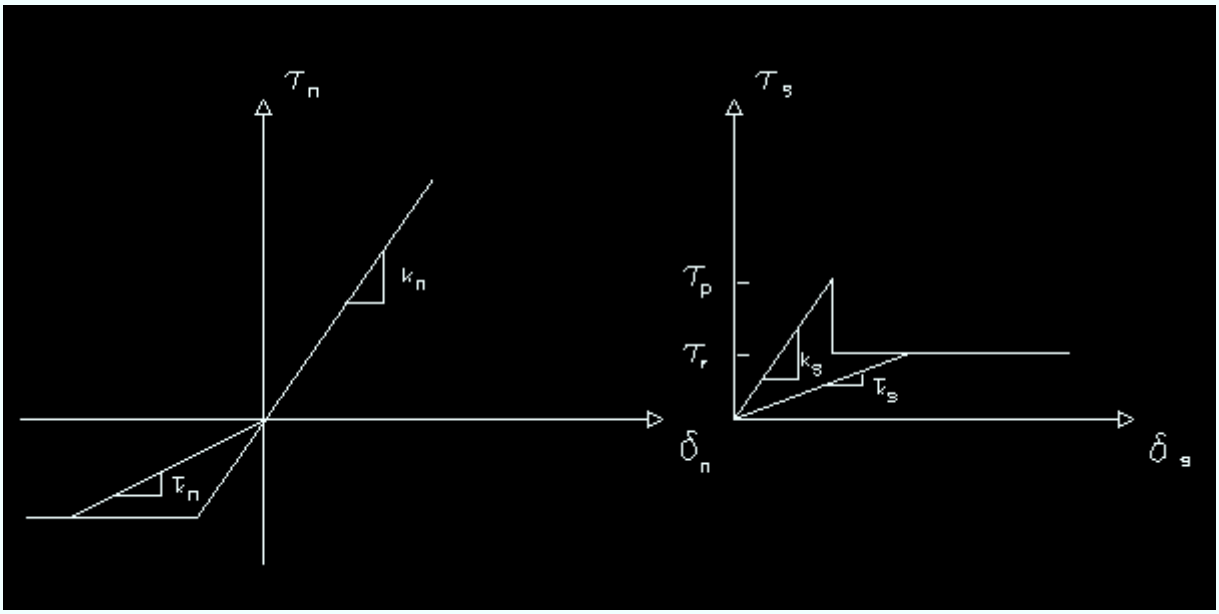


Figura 7.1.2- *Rappresentazione del metodo della rigidezza secante, definizione delle costanti equivalenti 'K_n, 'K_s*

Integrando tali espressioni, dato che i termini che includono il primo ordine $K_{n\times}$ L sono nulli si ottiene:

$$F_n = K_n \times D_{nx} L$$
$$F_s = K_s \times D_{sx} L \quad (7')$$
$$M = K_n \times \frac{L^3}{12} \quad (8')$$

ossia, in forma matriciale:

$$\begin{Bmatrix} F_n^p \\ F^p{}_s \\ M_\omega^p \end{Bmatrix} = \begin{bmatrix} K_n & 0 & 0 \\ 0 & K_s & 0 \\ 0 & 0 & K_\omega \end{bmatrix} \cdot \begin{Bmatrix} \Delta_n^p \\ \Delta^p{}_s \\ \Delta_\omega^p \end{Bmatrix} \quad (9)$$

dove:

$$K_n = K_{nx} L; K_s = K_{sx} L; Kw = K_{nx} \frac{L^3}{12}$$

Per convenienza, trasformiamo le forza di interfaccia F_n^P e F_s^P in F_x^P e F_y^P , passando rispettivamente dal sistema di coordinate locali *n-s* al sistema globale *X-Y* nel seguente modo:

$$\begin{Bmatrix} F_x^p \\ F_y^p \\ M^p \end{Bmatrix} = \begin{bmatrix} \cos\alpha & -\sin\alpha & 0 \\ \sin\alpha & \cos\alpha & 0 \\ 0 & 0 & 1 \end{bmatrix} \cdot \begin{Bmatrix} F_n^p \\ F_y^p \\ M^p \end{Bmatrix} \quad (10)$$

Le forze risultanti agenti su ogni faccia di un blocco devono soddisfare le condizioni di equilibrio date da:

$$\begin{Bmatrix} F_x^p \\ F_y^p \\ M^p \end{Bmatrix} = \sum_p^N \begin{bmatrix} -1 & 0 & 0 \\ 0 & -1 & 0 \\ r_y^{ap} & -r_x^{ap} & -1 \end{bmatrix} \cdot \begin{Bmatrix} F_x^p \\ F_y^p \\ M^p \end{Bmatrix} \quad (11)$$

dove *N* è il numero totale di facce del blocco. Le variabili f_x^a, f_y^a, m^a sono le forze ed i momenti di massa gravitazionali del blocco A. Combinano le equazioni 3, 4, 9, 10 e 11 otteniamo un legame tra forze e spostamenti del blocco A come di seguito riportato:

$$\begin{Bmatrix} f_x^a \\ f_y^a \\ m_\omega^a \end{Bmatrix} = \sum_p^N \begin{bmatrix} c_{11} & c_{12} & c_{13} \\ c_{21} & c_{22} & c_{23} \\ c_{31} & c_{32} & c_{33} \end{bmatrix} \cdot \left\{ \begin{bmatrix} 1 & 0 & -r_y^{bp} \\ 0 & 1 & r_x^{bp} \\ 0 & 0 & 1 \end{bmatrix} \cdot \begin{Bmatrix} u_x^b \\ u_y^b \\ \omega^b \end{Bmatrix} - \begin{bmatrix} 1 & 0 & -r_y^{ap} \\ 0 & 1 & r_x^{ap} \\ 0 & 0 & 1 \end{bmatrix} \cdot \begin{Bmatrix} u_x^a \\ u_y^a \\ \omega^a \end{Bmatrix} \right\} \quad (12)$$

la matrice *[c]* è data dal prodotto delle seguenti matrici:

$$\begin{bmatrix} -1 & 0 & 0 \\ 0 & -1 & 0 \\ r_y^{ap} & r_x^{ap} & -1 \end{bmatrix} \cdot \begin{bmatrix} \cos\alpha & -\sin\alpha & 0 \\ \sin\alpha & \cos\alpha & 0 \\ 0 & 0 & 1 \end{bmatrix} \cdot \begin{bmatrix} K_n & 0 & 0 \\ 0 & K_s & 0 \\ 0 & 0 & K_\omega \end{bmatrix} \cdot \begin{bmatrix} \cos\alpha & \sin\alpha & 0 \\ -\sin\alpha & \cos\alpha & 0 \\ 0 & 0 & 1 \end{bmatrix} \quad (13)$$

Facendo riferimento all' Eq. 12, per ogni blocco possiamo scrivere le tre equazioni di equilibrio delle forze e dei momenti, ottenendo un sistema di 3× N equazioni, per N blocchi, è espresso nel modo seguente:

$$\{f\} = [G] \times \{u\} \quad (14)$$

{ f } : è composta da f_x, f_y e m, per ogni blocco

{ u } : è composta da u_x, u_y ed w , per ogni blocco

[G]: è la matrice di rigidezza totale.

Quindi per ogni blocco abbiamo sei variabili le forze di massa f_x, f_y *e m* ed gl spostamenti u_x, u_y *e la rotazione w* , delle quali tre sono note cioè : f_x *ed m sono, uguali a zero.*
Risolvendo il sistema delle *3× N equazioni* si ricavano le *3× N incognite*.
Trovati gli spostamenti baricentrici di ogni blocco, tramite l'equazione 3 si possonc ricavare gli allungamenti delle molle tra due blocchi adiacenti. Da questi allungament tramite le relazioni *forze-allungamenti (Eq. 4 e 9)*, si possono ricavare le forze normal e tangenziali. Infine si possono ricavare le tensioni normali σ_n e tangenziali τ_s agent su ogni interfaccia di due blocchi, dividendo le forze trovate per l'area dell'interfaccia stessa, ossia:

$$\sigma_n = \frac{F_n}{L} \quad (15)$$

$$\tau_s = \frac{F_s}{L} \quad (16)$$

© GeoStru Software-SLOPE 8.0.1

Discrete Element Method for Slope Stability Analysis

By Ching S. Chang,[1] Member, ASCE

Abstract: Limit equilibrium methods for slope stability analysis do not, in general, satisfy the overall equilibrium conditions; they must make assumptions regarding the inclination and location of the interslice forces. An alternative slope analysis based on the discrete element method is presented to avoid these drawbacks. A slope in the present model is treated as comprised of slices that are connected by elastoplastic Winkler springs. By considering the conditions of compatibility, stresses on the mobilized surface can be obtained that are statically admissible and consistent with the material strength. The formulation of the method is presented and followed by a comparison of the method with limit equilibrium methods. Examples are also shown that demonstrate the applicability of the method to the analysis of progressive failure involving local yield and subsequent stress redistribution.

Introduction

In the limit equilibrium analysis of slope stability it is conjectured that the slope fails as a mass of soil sliding on a mobilized surface. The premise is that when a set of estimated stresses on the mobilized surface satisfies equilibrium conditions and is consistent with the strength of the material, this set of stresses provides an approximate solution that can be used for practical purposes to evaluate the overall factor of safety of the slope.

In most conventional slope stability methods, the soil mass is divided into a number of slices. The stress on the mobilized surface is estimated by employing the conditions of static equilibrium for each slice. However, the problem is indeterminate, and the conditions of static equilibrium are not sufficient for determining the stress on the mobilized surface. As a result, it is necessary to solve the problem by either neglecting part of the equilibrium conditions or by making assumptions as to the location and inclination of interslice forces. For example, the ordinary method of slices (Fellenius 1936) and Bishop's method (1955) do not satisfy the condition of overall force equilibrium while the infinite slope analysis (Fredlund and Krahn 1977), wedge analysis, and Janbu's (1954a) simplified method do not satisfy the condition of overall moment equilibrium. The more sophisticated methods attempt to satisfy all conditions of equilibrium by making additional assumptions regarding interslice forces (Spencer 1967; Morgenstern and Price 1965; Janbu 1957). These shortcomings, inherent in the limit equilibrium method, are unavoidable.

In recent years, despite the popularity of the limit equilibrium methods in engineering practice, the aforementioned shortcomings have been frequently raised in the assessment of these methods, e.g., in the investigations by Turnbull and Hvorslev (1967), Whitman and Bailey (1967), Wright et al. (1973), Duncan and Wright (1980), and Nash (1987).

---

[1]Prof. of Civ. Engrg., Univ. of Massachusetts, Amherst, MA 01003.

Note. Discussion open until May 1, 1993. To extend the closing date one month, a written request must be filed with the ASCE Manager of Journals. The manuscript for this paper was submitted for review and possible publication on May 11, 1991. This paper is part of the *Journal of Geotechnical Engineering*, Vol. 118, No. 12, December, 1992. ©ASCE, ISSN 0733-9410/92/0012-1889/$1.00 + $.15 per page. Paper No. 1839.

In contrast to the simple procedures for obtaining the stresses on a mobilized surface used in the limit equilibrium methods, more rigorous methods are desirable, such as finite element techniques. With advances in computer technology, the extensive computational effort associated with finite element methods is no longer a major concern. However, finite element methods require information about the initial stress state existing in the slope, a correct constitutive model, and correct parameters for the constitutive model. This greatly increases the complexity of analysis and the uncertainty of its results.

The purpose of this paper is to investigate a more direct and simple approach. The present approach considers the conditions of compatibility between the slices of which the slope is comprised. The interfaces between the slices are elastoplastic in nature. This model, a slight extension of the conventional right-plastic assumption, permits a solution that satisfies all equilibrium conditions without requiring any assumptions regarding interslice forces.

The analytic technique presented in this paper falls within the class of discrete element methods. Compared with other discrete element methods, e.g., those used by Cundall (1971) and Shi (1988) in the analysis of the movement of rock blocks, the present method is similar in concept but different in both formulation and solution procedure.

In what follows, the formulation of the present method for slope analysis is presented. The present method is compared with several conventional slope stability methods, such as the simplified Bishop method, Janbu's method, and Spencer's method. Application of the present method is also illustrated for the progressive failure of a slope with brittle soil. Finally, a parametric comparison is shown for varying degrees of brittleness of soil to illustrate their relative effect on the overall factor of safety.

Discrete Element Model for Slope Analysis

Interface between Slices

For a slope divided into n slices there are in general $5n - 2$ unknowns: n for the normal forces on the base of the slice; n for the positions of the normal forces; $n - 1$ for the interslice forces; $n - 1$ for the inclination of the interslice forces; $n - 1$ for the height of the interslice forces; and 1 for the factor of safety used to relate shear forces to the normal forces.

On the other hand, there are only $3n$ equations of static equilibrium available (vertical, horizontal, and moment equilibrium). Thus $2n - 2$ assumptions must be made for the problem to be rendered solvable. A brief summary of the assumptions made in various limit equilibrium methods for slope stability analysis is given in Table 1. It can be seen that most methods do not completely satisfy equilibrium conditions and that all methods involve assumptions about interslice forces.

To avoid the shortcomings of limit equilibrium slope stability methods, the present method accounts for the compatibility between slices so that sufficient additional equations can be provided to solve the problem. For this purpose, each slice and its neighboring slices or base are linked together by Winkler springs, as shown in Fig. 1. One set of springs is in the normal direction to simulate the normal stiffness. The other set is in the shear direction to simulate the sliding resistance at the interface.

The behavior of the normal and shear springs is elastoplastic, as shown in Fig. 2. The normal springs do not yield in compression, but they yield

TABLE 1. Summary of Conventional Methods of Slope Analysis

Methods (1)	Overall moment equilibrium (2)	Overall force equilibrium (3)	Assumptions about interslice forces (4)
Bishop (1955)	X	—	Horizontal
Wedge analysis	—	X	Define inclination
Infinite slope (Skempton and Delory 1957)	—	X	Parallel to slope
Ordinary (Fellenius 1936)	X	—	Parallel to base of each slice
Janbu simplified (1956)	—	X	Horizontal
Lowe and Karafiath (1960)	—	X	Define inclination
Spencer (1967)	X	X	Constant inclination
Morgenstern and Price (1965)	X	X	Assumed function of location
Janbu rigorous (1957)	X	X	Define thrust line
Frelund and Krahn GLE (1977)	X	X	Assumed function of location
Law and Lumb (1978)	X	X	Define inclination

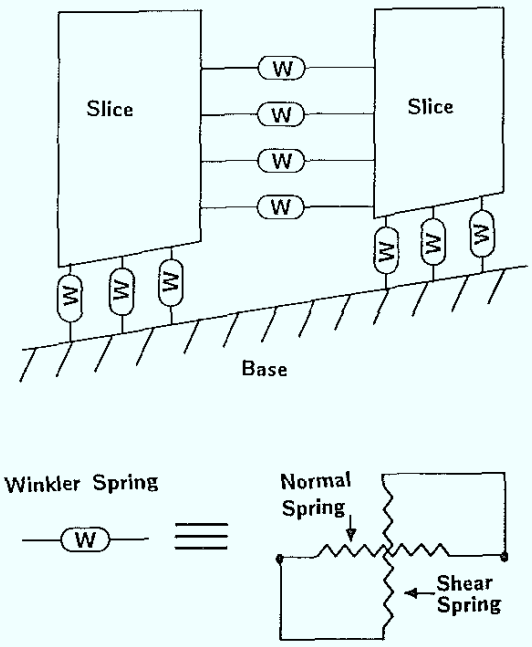


FIG. 1. Schematic Figure of Winkler Springs at Interface between Two Adjacent Slices or between Slice and Immovable Base

in tension, with a small tensile capacity for cohesive soil (tension cutoff) and no tensile capacity for frictional soil.

The shear springs yield when the shear strength is reached. For brittle soil, the peak strength of the shear springs is determined by

$$\tau_p = c_p + \sigma_n \tan \phi_p \quad \ldots\ldots (1)$$

After the peak strength is reached, the strength decreases with increasing strain and approaches the residual shear strength given by

$$\tau_r = c_r + \sigma_n \tan \phi_r \quad \ldots\ldots (2)$$

For simplicity, in the following analysis, it is assumed that after reaching the peak strength, the soil resistance drops immediately to the residual strength value, as shown in Fig. 2.

For plastic nonbrittle soil, the strength does not reduce at large shear deformation; thus, the residual strength has the same value as the peak strength.

Method of Analysis

The formulation of the present method follows that of previous research (Chang and Misra 1989; Chang and Ma 1990) on the mechanics of discrete particulates. Let $\mathbf{u}_i^a$, $\mathbf{u}_i^b$, and $\boldsymbol{\omega}^a$, $\boldsymbol{\omega}^b$ represent the translations and rotations of slice A and slice B, respectively. Let P be the midpoint of the interface between these slices. The displacement of slice B relative to slice A, at point P, is then expressed as follows:

$$\begin{Bmatrix} \boldsymbol{\Delta}_x^p \\ \boldsymbol{\Delta}_y^p \\ \boldsymbol{\Delta}_\omega^p \end{Bmatrix} = \begin{bmatrix} 1 & 0 & -\mathbf{r}_y^{bp} \\ 0 & 1 & \mathbf{r}_x^{bp} \\ 0 & 0 & 1 \end{bmatrix} \begin{Bmatrix} \mathbf{u}_x^b \\ \mathbf{u}_y^b \\ \boldsymbol{\omega}^b \end{Bmatrix} - \begin{bmatrix} 1 & 0 & -\mathbf{r}_y^{ap} \\ 0 & 1 & \mathbf{r}_x^{ap} \\ 0 & 0 & 1 \end{bmatrix} \begin{Bmatrix} \mathbf{u}_x^a \\ \mathbf{u}_y^a \\ \boldsymbol{\omega}^a \end{Bmatrix} \quad \ldots\ldots\ldots\ldots (3)$$

where $\mathbf{r}_i^{ap}$ = the vector joining the centroid of the slice to location P. If, however, the neighbor of slice A has an immobile base, the values of $\mathbf{u}_x^b$, $\mathbf{u}_y^b$, and $\boldsymbol{\omega}^b$ are taken as zero.

Let $\mathbf{n}_i^p$ be an inward vector normal to the side face of slice A at point P, defined as $\mathbf{n}_i^p = (\cos\alpha, \sin\alpha)$, where α = the angle between the x-axis and the vector $\mathbf{n}_i^p$. The vector $\mathbf{s}_i^p$ perpendicular to $\mathbf{n}_i^p$ is defined as $(-\sin\alpha, \cos\alpha)$. Thus the displacement vector on the left side of (1) can be transformed from $x - y$ coordinates to the local $n - s$ coordinates as follows:

$$\begin{Bmatrix} \boldsymbol{\Delta}_n^p \\ \boldsymbol{\Delta}_s^p \\ \boldsymbol{\Delta}_\omega^p \end{Bmatrix} = \begin{bmatrix} \cos\alpha & \sin\alpha & 0 \\ -\sin\alpha & \cos\alpha & 0 \\ 0 & 0 & 1 \end{bmatrix} \begin{Bmatrix} \boldsymbol{\Delta}_x^p \\ \boldsymbol{\Delta}_y^p \\ \boldsymbol{\Delta}_\omega^p \end{Bmatrix} \quad \ldots\ldots\ldots\ldots\ldots\ldots\ldots\ldots (4)$$

Due to the relative movements of two neighboring slices as shown in Fig. 3, at any point P' on the interface, the spring stretch in the normal direction $\boldsymbol{\delta}_n$ and in the shear direction $\boldsymbol{\delta}_s$ are given by

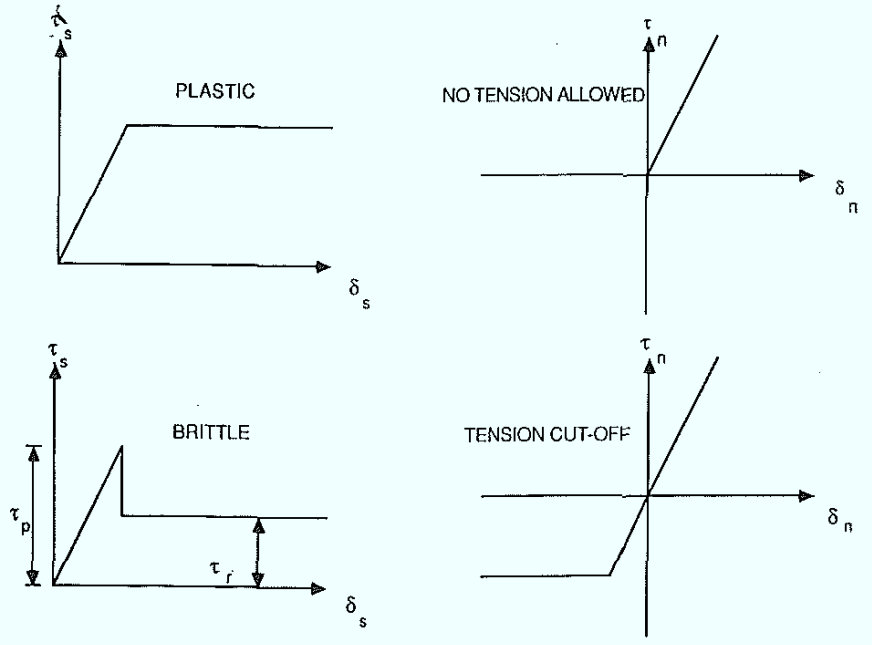


FIG. 2. Behavior of Normal and Shear Winkler Springs

$$\delta_n = \Delta_n + l\Delta_\omega \quad \ldots\ldots (5a)$$

$$\delta_s = \Delta_s \quad \ldots\ldots (5b)$$

where l = distance from the center point P to point P'.

As a result of spring stretch, normal and shear stresses on the slice interface are generated as shown in Fig. 3. These stresses on the interface can be integrated to obtain the resultant forces and moment as follows:

$$\mathbf{F}_n = \int_{-L/2}^{L/2} k_n \delta_n \, dl = \int_{-L/2}^{L/2} k_n \Delta_n \, dl + \int_{-L/2}^{L/2} k_n l \Delta_\omega \, dl \quad \ldots\ldots (6)$$

$$\mathbf{F}_s = \int_{-L/2}^{L/2} k_s \delta_s \, dl = \int_{-L/2}^{L/2} k_s \Delta_s \, dl \quad \ldots\ldots (7)$$

$$\mathbf{M} = \int_{-L/2}^{L/2} k_n l \delta_n \, dl = \int_{-L/2}^{L/2} k_n l \Delta_n \, dl + \int_{-L/2}^{L/2} k_n l^2 \Delta_\omega \, dl \quad \ldots\ldots (8)$$

where k_n = spring constant per unit length of the normal spring; k_s = spring constant per unit length of the shear spring; and L = length of the interface.

Note that the springs are elastoplastic. The value of these spring constants therefore are obtained based on their stress-displacement relationship, shown in Fig. 2.

For a nonyield interface, the elastic spring constants k_n and k_s are used. For a yield interface, elastic constants are no longer applicable, and a method that considers the nonlinearity of the problem is required. In this regard, a secant stiffness method is employed. The equivalent spring constant $\bar{k}_n$ and $\bar{k}_s$ for a yield interface can be obtained that corresponds to the deformation of the interface, as shown in Fig. 4. Since the deformation of the interface is unknown before gravity loading is applied, an iterative procedure is carried out until the shear stresses at all the bases of the slices completely satisfy the stress-displacement relationship.

With the yielding of springs taken into consideration, the excess stress of the failed slice is distributed among the neigbtoring slices. This redistribution of stress causes a local failure to propagate.

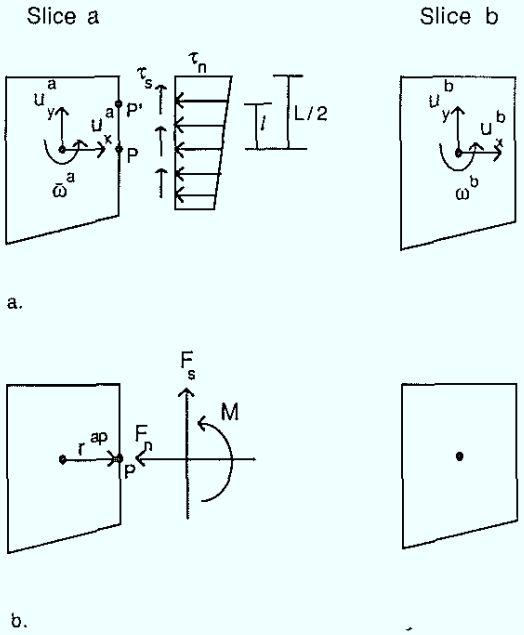


FIG. 3. (*a*) Shear and Normal Stresses between Adjacent Slices Due to Their Relative Movement; (*b*) Equivalent Forces and Moments between Adjacent Slices

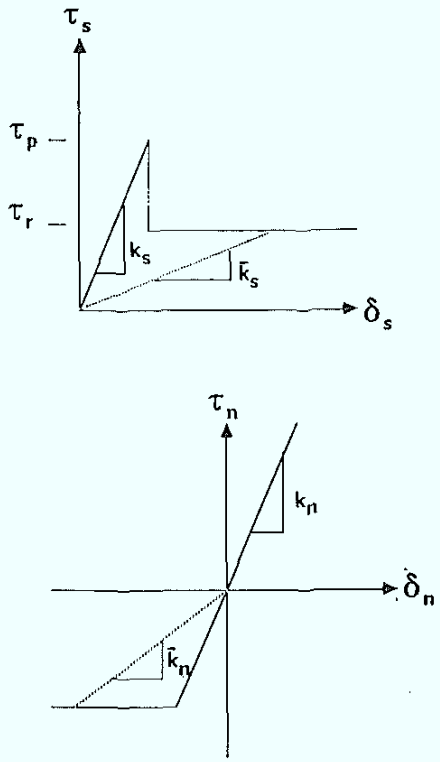


FIG. 4. Secant Stiffness Method for Obtaining k_n and k_s

Note that the terms on the right-hand side of (6–8) involving the first order of $k_n l$ are equal to zero. Integrating these expressions, we obtain

$$\begin{Bmatrix} \mathbf{F}_n^p \\ \mathbf{F}_s^p \\ \mathbf{M}^p \end{Bmatrix} = \begin{bmatrix} K_n & 0 & 0 \\ 0 & K_s & 0 \\ 0 & 0 & K_\omega \end{bmatrix} \begin{Bmatrix} \boldsymbol{\Delta}_n^p \\ \boldsymbol{\Delta}_s^p \\ \boldsymbol{\Delta}_\omega^p \end{Bmatrix} \quad \ldots\ldots\ldots\ldots\ldots\ldots\ldots\ldots\ldots\ldots\ldots\ldots (9)$$

where $K_n = k_n L$; $K_s = k_s L$; and $K_\omega = k_n L^3/12$.

For convenience, the side forces F_n^p and F_s^p in the local coordinate system are transformed to $\mathbf{F}_x^p$ and $\mathbf{F}_y^p$ in the global coordinate system as shown in the following:

$$\begin{Bmatrix} \mathbf{F}_x^p \\ \mathbf{F}_y^p \\ \mathbf{M}^p \end{Bmatrix} = \begin{bmatrix} \cos\alpha & -\sin\alpha & 0 \\ \sin\alpha & \cos\alpha & 0 \\ 0 & 0 & 1 \end{bmatrix} \begin{Bmatrix} \mathbf{F}_n^p \\ \mathbf{F}_s^p \\ \mathbf{M}^p \end{Bmatrix} \quad \ldots\ldots\ldots\ldots\ldots\ldots\ldots\ldots\ldots\ldots (10)$$

The forces acting on all sides of a slice should satisfy the equilibrium requirement, given by

$$\begin{Bmatrix} \mathbf{f}_x^a \\ \mathbf{f}_y^a \\ \mathbf{m}^a \end{Bmatrix} = \sum_p^N \begin{bmatrix} -1 & 0 & 0 \\ 0 & -1 & 0 \\ \mathbf{r}_y^{ap} & -\mathbf{r}_x^{ap} & -1 \end{bmatrix} \begin{Bmatrix} \mathbf{F}_x^p \\ \mathbf{F}_y^p \\ \mathbf{M}^p \end{Bmatrix} \quad \ldots\ldots\ldots\ldots\ldots\ldots\ldots\ldots\ldots\ldots (11)$$

where N = the total number of sides of the slice. The force $\mathbf{f}_y^a$ is the weight of the slice acting through its centroid. The body force $\mathbf{f}_x^a$ and moment m^a of the slice are usually equal to zero.

Combining (11), (10), (9), (4) and (3), a relationship is obtained between the forces and the movements of the slice in the following form:

$$\begin{Bmatrix} \mathbf{f}_x^a \\ \mathbf{f}_y^a \\ \mathbf{m}^a \end{Bmatrix} = \sum_p^N \begin{bmatrix} c_{11} & c_{12} & c_{13} \\ c_{21} & c_{22} & c_{23} \\ c_{31} & c_{32} & c_{33} \end{bmatrix} \left(\begin{bmatrix} 1 & 0 & -\mathbf{r}_y^{bp} \\ 0 & 1 & \mathbf{r}_x^{bp} \\ 0 & 0 & -1 \end{bmatrix} \begin{Bmatrix} \mathbf{u}_x^b \\ \mathbf{u}_y^b \\ \boldsymbol{\omega}^b \end{Bmatrix} \right.$$

$$- \begin{bmatrix} 1 & 0 & -\mathbf{r}_y^{ap} \\ 0 & 1 & \mathbf{r}_x^{ap} \\ 0 & 0 & 1 \end{bmatrix} \begin{Bmatrix} \mathbf{u}_x^a \\ \mathbf{u}_y^a \\ \boldsymbol{\omega}^a \end{Bmatrix} \Bigg) \quad \ldots\ldots\ldots\

$$\lambda = \frac{\gamma H}{c} \tan \phi \quad \ldots\ldots\ldots\

Winkler springs at the interfaces. Although any values of k_n and k_s would result in a statically admissible solution, more rational values of k_n and k_s would lead to a more realistic solution. From the results of the analysis of the homogeneous embankments, it was found that the solution is a function of the ratio k_n/k_s rather than their individual values. Table 2 shows the variation in the computed factors of safety, with k_n/k_s ranging from 1 to 10. The ratio of the stiffness in the normal and shear directions of an interface, k_n/k_s, can be estimated by analogy to the ratio of Young's modulus to the shear modulus of the material. For an isotropic elastic material, this ratio is given by $2(1 + \nu)$. The value of k_n/k_s can thus be selected based upon the estimated Poisson's ratio of the soil. For example, the ratio k_n/k_s of undrained saturated clay (i.e., $\nu = 0.5$) is 3. For the range of Poisson's ratio ν from 0 to 0.5, the practical range of k_n/k_s is from 2 to 3.

For comparison with other methods, e.g., the ordinary method, Spencer's method, Janbu's simplified and rigorous methods, and the Morgenstern-Price method, the present method is employed to compute the example problem shown in Fig. 6. The slope is 2 on 1, 40 ft high, $\phi' = 20$, $c' = 600$ lb/sq ft (28.73 kN/m^2) (29 kPa). Safety factors are computed for two conditions: (1) The drained condition; and (2) with pore pressure taken into consideration (the ratio of pore pressure to overburden stress $r_u = 0.25$). This illustration is not meant to be a comprehensive comparison of methods but rather a typical example. The computed factors of safety for various methods are shown in Table 3.

Comparisons of the predicted results obtained from the present method and other methods are discussed in two areas: (1) The factors of safety; and (2) the stress on the mobilized surface.

1. Factors of safety. Comparing the computed factors of safety in Table 2, the present method predicts smaller factors of safety for slopes with frictional material, especially for steep slopes, indicating that Bishop's method may give unconservative predictions for these conditions. In Table 3, the factors of safety obtained from various methods for the first case vary from 1.92 to 2.085 and for the second case from 1.607 to 1.779. The present method tends to predict lower factors of safety than most of the limit equilibrium methods. The differences in safety factors shown in these few examples are not insignificant. Indeed, the results of these differences could be drastic in some cases, based on the observation by Whitman and Bailey

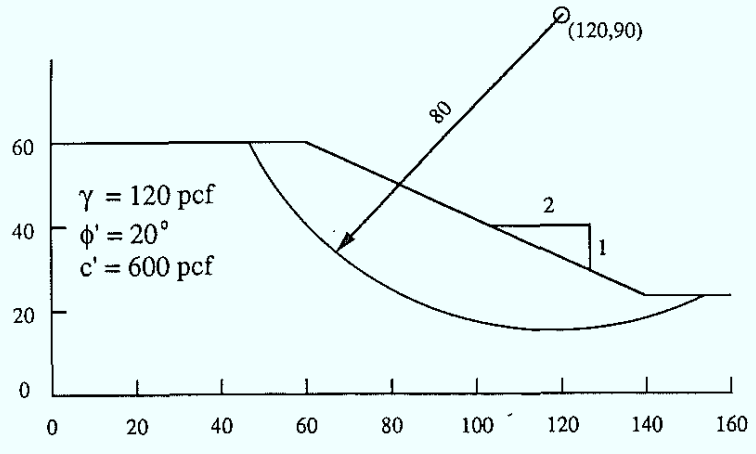


FIG. 6. Configuration of Slope Used in Example 2

TABLE 3. Computed Factors of Safety for Various Methods

Case number (1)	Example problem[a] (2)	Ordinary method (3)	Simplified Bishop's method (4)	Spencer's Method			Janbu's simplified method (8)	Janbu's rigourous method[b] (9)	Morgenstern-Price Method $f(x)$ = constant		Present study (12)
				f (5)	θ (6)	λ (7)			F (range) (10)	λ (range) (11)	
1	Simple 2:1 slope; 40 ft (12 m) high; $\phi' = 20$; $c' =$ 600 psf (29 kPa)	1.928	2.080	2.073	14.81	0.237	2.041	2.008	2.076–2.085	0.254–0.318	1.92
2	Same as case 1 except with $r_u = 0.25$	1.607	1.766	1.761	14.33	0.255	1.735	1.708	1.765–1.779	0.244–0.432	1.68

[a]Width of the slice is 0.5 ft (0.3 m), and the tolerance on the nonlinear solutions is 0.001.
[b]The line of thrust is assumed at 0.333.

(1967) and Leshchinsky (1990) that the sensitivity of factors to the static assumption is significant.

2. Stress on the mobilized surface. The computed shear stresses along the mobilized surface from various methods differ significantly. For example, as shown in Fig. 7, the shear stress calculated by the present method is generally lower than that determined by Bishop's method in the central portion and higher at the toe and heel of the mobilized surface. However, the normal stress distribution along the surface shows good agreement, as shown in Fig. 8.

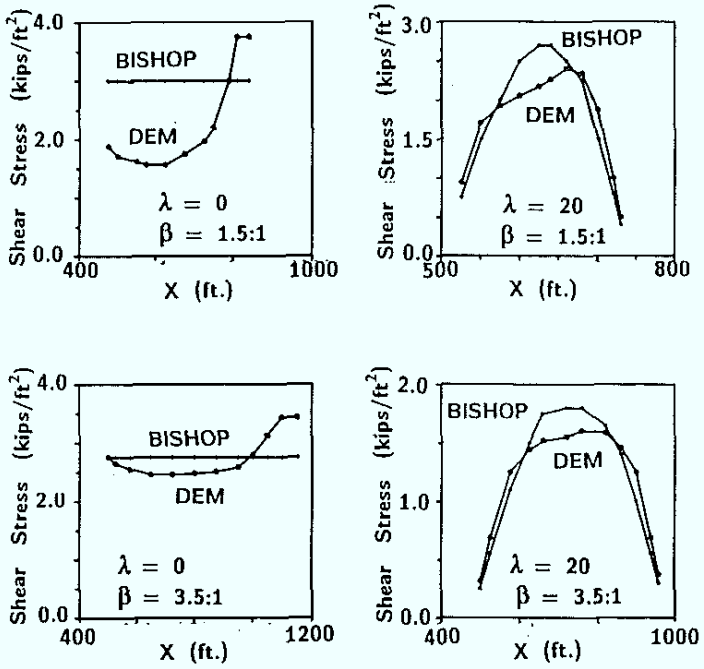


FIG. 7. Shear Stress Distribution along Mobilized Surface Obtained from Bishop's Method and Present Method

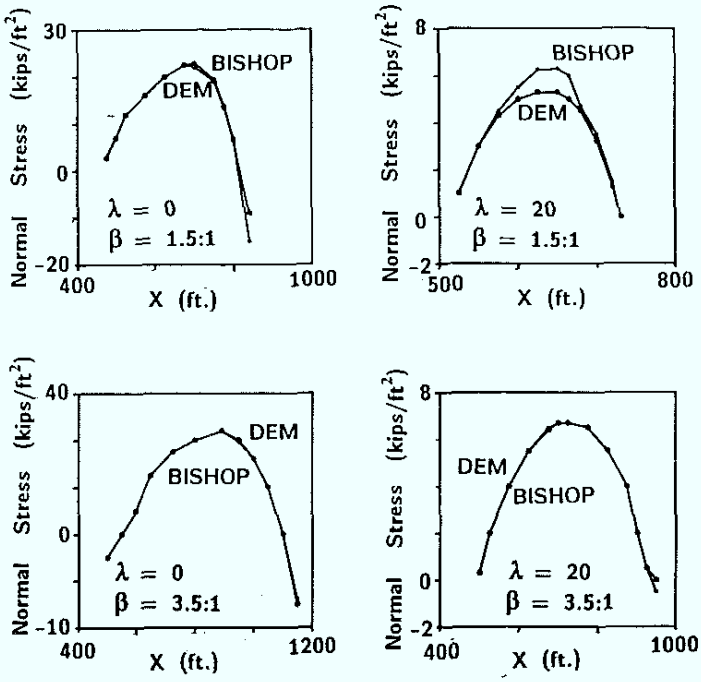


FIG. 8. Normal Stress Distribution along Mobilized Surface Obtained from Bishop's Method and Present Method

In conventional slope stability methods, it is assumed that the factors of safety are the same for all slices on the mobilized surface. The present discrete element approach, however, is not limited by this assumption. Therefore the present method is capable of predicting variation in the factors of safety, as shown in Fig. 9, along the mobilized surface. The computed results in Fig. 9 are in agreement with results obtained from field studies and from the finite element analysis of an embankment (Lo and Lee 1973) that show that the toe of a slope fails in shear, while the heel fails in tension. The initiation of failure begins at the toe and heel, and the local failure propagates from these regions toward the central portion of the slope. It is noted that the progressive failure in this example takes place in slopes made of plastic soil (see Fig. 2), which do not show a reduction of shear strength after reaching peak strength.

Due to the consideration of the elastoplastic Winkler springs, the present model accounts for the postyielding behavior; when the shear stress of one slice exceeds the strength on the mobilized surface, the excess stress is distributed to the neighboring slices. The capability of modeling such a mechanism of progressive failure in the slope analysis leads to a more realistic prediction of the stress distribution along the mobilized surface. The practical consequences are as follows.

1. The present model gives a more accurate prediction of factors of safety.
2. The present model, which considers progressive failure, leads to lower factors of safety than those obtained from most limit equilibrium methods.
3. The present model is useful for brittle soil with low residual strength where the progressive failure mechanism is a critical factor.

Progressive Failure Analysis for Brittle Soil

The mechanism of progressive failure is known to have significant effects on the overall factor of safety for brittle soil, which shows strength reduction after yielding. Failure induced by this type of mechanism has been frequently

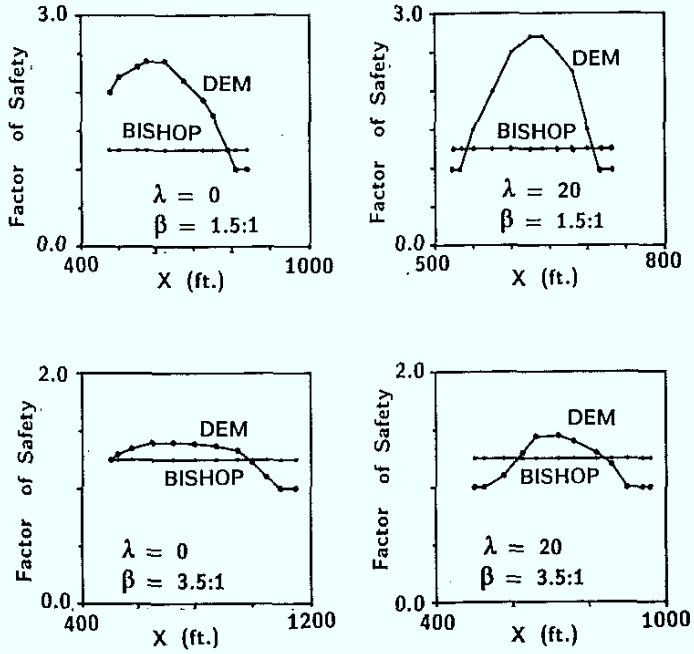


FIG. 9. Factor of Safety along Mobilized Surface Obtained from Bishop's Method and Present Method

accounted for by the instability of slopes (Bjerrum 1967; Burland et al. 1977). However, most analytical methods developed for progressive failure analysis based on limit equilibrium methods have two inherent shortcomings: (1) The predicted shear stress distribution is not reliable using static assumptions; and (2) the manner of stress redistribution, which cannot be described by force equilibrium alone, must be analyzed with an empirical procedure. The present method, which treats the interface of slices as elastoplastic in nature, can avoid these shortcomings and effectively model the mechanism of progressive failure. To demonstrate the model performance, an example is shown for case 4 of Fig. 5 ($\lambda = 20$, $\beta = 3.5$), using residual strength parameters $\phi_r = 0.55\phi_p$, and $c_r = c_p$.

Fig. 10 shows the variation of factors of safety along the mobilized surface at successive iteration stages. It may be observed that at the initial stage, the variation of safety factors indicates failure at the toe and heel of the mobilized surface. At successive stages, due to strength reduction and stress redistribution, the computed factors of safety indicate that the mobilized surface fails progressively from the toe and heel to the central portion, leading to a complete sliding of the soil mass. In this case, the driving shear stress due to the weight of the soil mass exceeds the capacity of the resisting shear strength. Therefore, the overall factor of safety is less than one.

Similar behavior of progressive failure leading to complete sliding is also found in the analysis of a valley slope of the River Lune, near Middleton-in-Teesdale, England, as shown in Fig. 11. The slope described by Skempton and Brown (1961) has an inclination of 28°, a height of 12.8 m, and consists of soils with a unit weight equal to 21.8 kN/m^3. The peak-strength parameters are given as $\phi_p = 32°$ and $c_p = 8.6$ kN/m^2. The residual strength in this case is given by Skempton and Brown as $\phi_r = \phi_p$ and $c_r = 0$. The analysis was performed with a pore-pressure parameter value r_u equal to 0.35.

It was found that the locations and inclinations of the interslice forces of the slope computed using the present analysis are significantly different from those assumed by Law and Lumb (1978), as given in Fig. 12.

To show the effect of brittleness on the overall factor of safety, a parametric comparison was performed. For convenience, a frictional brittleness index I_ϕ is defined as

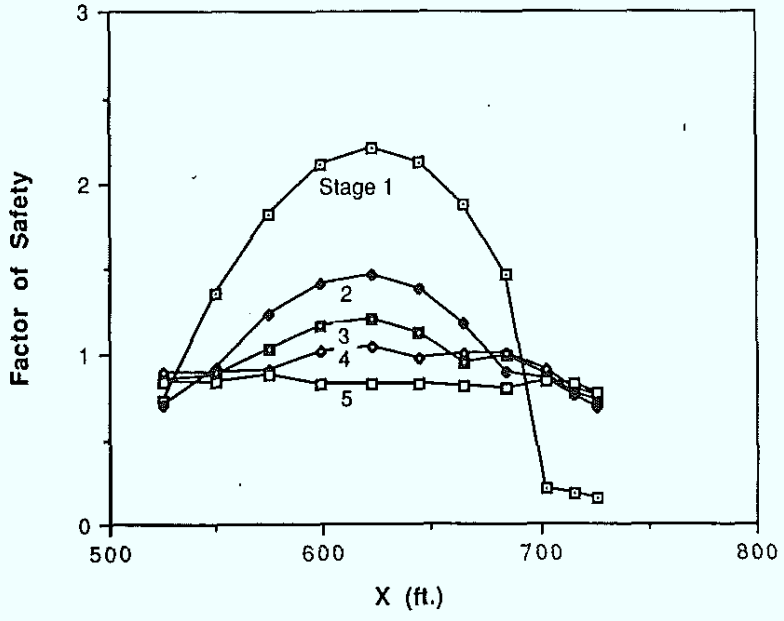


FIG. 10. Factor of Safety Distribution along Failure Surface at Successive Iteration Stages

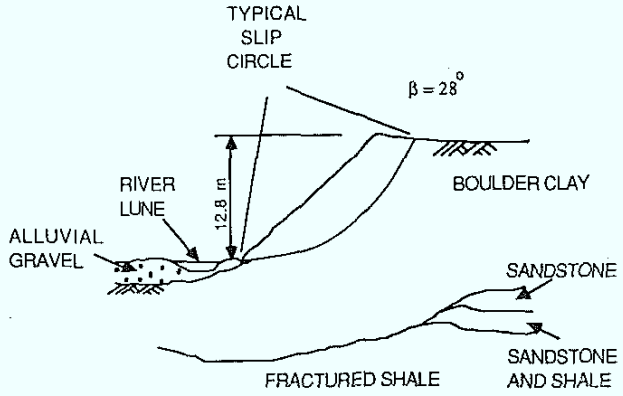
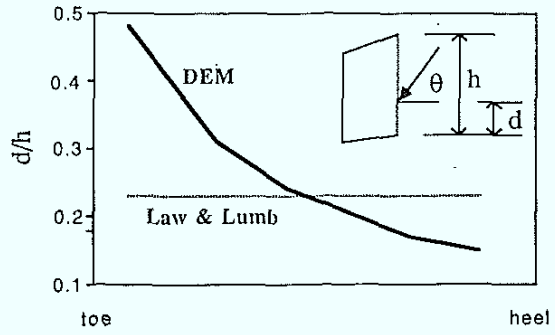


FIG. 11. River Lune Slope



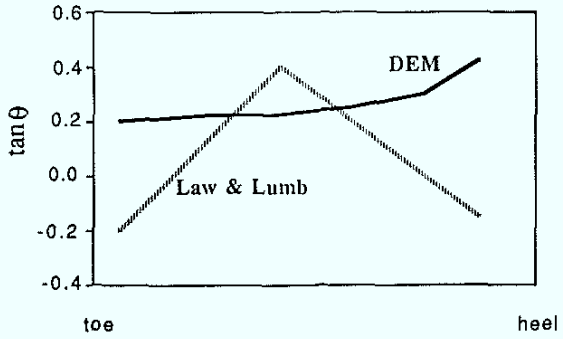


FIG. 12. Computed Locations and Inclinations of Interslice Forces by Present Method Compared with that Assumed in Method of Law and Lumb (1978)

$$I_\phi = \frac{\phi_p - \phi_r}{\phi_p} \quad \ldots\ldots\ldots\

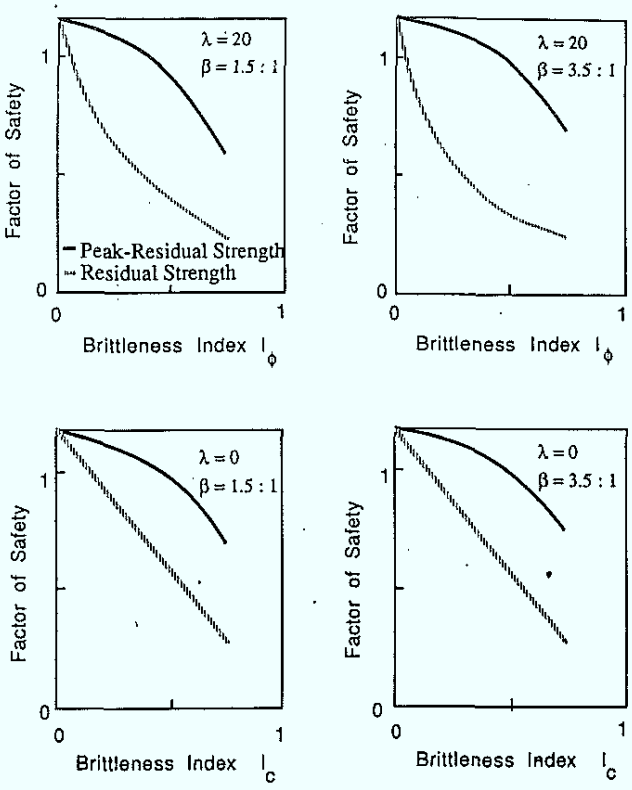


FIG. 13. Effect of Brittleness on Overall Factor of Safety

the factors of safety are computed with various values of I_c and plotted using a solid line in Fig. 13. For purposes of comparison, factors of safety for various values of I_c are also computed using only the residual soil strength $c_p = c_r = 3{,}319\ (1 - I_c)$ psf. This condition, plotted using a dashed line in Fig. 13, is the lower bound solution for this case.

For case 3, $\lambda = 20$, $\beta = 1.5{:}1$, and $c_r = c_p$. After the frictional strength of soil reaches the peak strength ϕ_p (i.e., 14.8°), it is reduced to ϕ_r, which is equal to $14.8°\ (1 - I_\phi)$. Using the present model, the factors of safety are computed with various values of I_ϕ and plotted using a solid line in Fig. 13. For purposes of comparison, the residual strength condition is also analyzed for case 3 by assuming $\phi_p = \phi_r = 14.8°\ (1 - I_\phi)$. The factor of safety plotted using a dashed line in Fig. 13 is the lower bound solution for this case. Similar results are also plotted for cases 2 and 4.

Fig. 13 summarizes the effect of brittleness on the overall factor of safety. Due to a reduction in the residual shear strength, the factors of safety decrease with an increasing brittleness index. The lower bound solutions of factor of safety are significantly overestimated compared to the predictions obtained from the present method.

Conclusion

Due to the nature of limit equilibrium analysis, all conventional methods for slope stability analysis must make assumptions with regard to the interslice forces. The current approach, based on the discrete element method, provides a method of estimating the stresses on a mobilized surface that is both simpler and more direct. A slope, in the present method, is treated as comprised of slices connected by elastoplastic Winkler springs. Important features of the model are summarized as follows:

1. The present method is theoretically more rigorous. The consideration

of elastoplastic springs yields a statically deterministic system and facilitates the treatment of stress redistribution along the mobilized surface. The obtained solution is both kinematically and statically admissible. The present model is a more rigorous alternative to limit equilibrium methods for slope analysis.

2. The present method is simpler than some conventional methods. The present model is simpler in the sense that no experience is required for making reasonable assumptions regarding the locations and inclinations of interslice forces, which is required by some of the conventional rigorous methods, such as Spencer's method, Janbu's rigorous method, and the Morgenstern-Price method.

3. The present method predicts lower factors of safety in some cases. In the examples given in this paper, the present method predicts lower factors of safety for slopes with frictional material, especially for steep slopes. The present method tends to predict lower factors of safety than some of the limit equilibrium methods. This may be due to consideration of the progressive failure mechanism in the present method.

4. The present method is useful in progressive failure analysis. As described in the section on progressive failure, the present method, in contrast to the limit equilibrium methods, is capable of modeling postyielding behavior. The present method permits consideration of both the peak and residual strength of the material which permits the determination of the region of the initiation of local yield and the subsequent stress redistribution. Therefore, the present model is a potentially useful tool for the stability analysis of slopes susceptible to progressive failure in brittle soil.

APPENDIX. REFERENCES

Bishop, A. W. (1955). "The use of slip circle in the stability analysis of slopes." *Geotechnique*, 5(1), 7–17.

Bjerrum, L. (1967). "Progressive failure in slopes of overconsolidated plastic clay shales." *J. Soil Mech. Found. Div.*, ASCE, 93(5), 3–49.

Burland, J. B., Longworth, T. I., and Moore, J. F. A. (1977). "A study of ground movement and progressive failure caused by deep excavation in Oxford clay." *Geotechnique*, 27(4), 557–591.

Chang, C. S., and Ma, L. (1990). "Modeling of discrete granulates as micropolar continuum." *J. Engrg. Mech.*, ASCE, 116(12), 2703–2721.

Chang, C. S., and Misra, A. (1990). "Computer simulation and modelling of mechanical properties of particulates." *J. Comput. Geotechniques*, 7(4), 269–287.

Cundall, P. A. (1971). "A computer model for simulating progressive, large-scale movements in block rock systems." *Proc. Int. Symp. on Rock Fracture*, Nancy, France, vol. 1, 8–17.

Duncan, J. M., and Wright, S. G. (1980). "The accuracy of equilibrium methods of slope stability analysis." *Engrg. Geol.*, Amsterdam, the Netherlands, 16(1/2), 5–17.

Fellinius, W. (1936). "Calculation of the stability of earth dams." *Proc. Second Congress on Large Dams*, 4, 445–463.

Fredlund, D. G., and Krahn, J. (1977). "Comparison of slope stability methods of analysis." *Can. Geotech. J.*, 14(3), 429–439.

Janbu, N. (1954a). "Application of composite slip surfaces for stability analysis." *European Conf. on Stability of Earth Slopes*, 3, 43–49.

Janbu, N. (1954b). "Stability analysis of slopes with dimensionless parameters." *Harvard Soil Mechanics Series 46*, Harvard Univ., Cambridge, Mass., 8–11.

Janbu, N. (1957). "Earth pressure and bearing capacity by generalized procedure of slices." *Proc. Fourth Int. Conf. Soil Mechanics*, 2, 207–212.

Law, K. T., and Lumb, P. (1978). "A limit equilibrium analysis of progressive failure in the stability of slopes." *Can. Geotech. J.*, 15(1), 113–122.
Leshchinsky, D. (1990). "Slope stability analysis: generalized approach." *J. Geotech. Engrg.*, ASCE, 116(5), 851–867.
Lo, K. Y., and Lee, C. F. (1973). "Stress analysis and slope stability in strain softening soils." *Geotechnique*, 23(1), 1–11.
Lowe, J., and Karafiath, L. (1960). "Stability of earthdams upon drawdown." *Proc. First Pan-American Conf. on Soil Mechanics and Foundation Engrg.*, 2, 537–552.
Morgenstern, N. R., and Price, V. E. (1965). "The analysis of the stability of general slip surfaces." *Geotechnique*, 15(1), 79–93.
Nash, D. T. F. (1987). "A comprehensive review of limit equilibrium methods of slope stability analysis." *Slope stability*, M. G. Anderson and K. S. Richards, ed., John Wiley, New York, N.Y., 11–75.
Shi, G. H. (1988). "Discontinuous deformation analysis: A new numerical model for the static and dynamics of block systems." PhD thesis, Univ. of California, Berkeley, Calif.
Skempton, A. W., and Brown, J. D. (1961). "A landslide in boulder clay at Selset, Yorkshire." *Geotechnique*, 11(4), 280–293.
Skempton, A. W., and Delory, F. A. (1957). "Stability of natural slopes in London clay." *Proc. Fourth Int. Conf. Soil Mechanics*, 2, 378–381.
Spencer, E. (1967). "A method of analysis of the stability of embankments assuming parallel interslice forces." *Geotechnique*, 17(1), 11–26.
Turnbull, W. J., and Hvorslev, M. L. (1967). "Special problems in slope stability." *J. Soil Mech. Found. Div.*, ASCE, 93(4), 499–528.
Whitman, R. V., and Bailey, W. A. (1967). "Use of computers for slope stability analysis." *J. Soil Mech. Found. Div.*, ASCE, 93(4), 475–498.
Wright, S. G., Kulhawy, F. H., and Duncan, J. M. (1973). "Accuracy of equilibrium slope stability analysis." *J. Soil Mech. Found. Div.*, ASCE, 99(10), 783–791.